Global Biogeochemical Cycles

RESEARCH ARTICLE
10.1029/2023GB007749

Changes in Dissolved Inorganic Carbon Across Yangtze River Regulated by Dam and River-Lake Exchange

Chu Zhao[1], Chuan Wang[1], Jianhong Li[1,2], Lize Meng[1], Jingya Xue[1], Yang Gao[3], Tao Huang[1], Yixin Bai[1], Shuaidong Li[1], Hao Yang[1], Kun Shi[4], Yuanhui Xu[1], and Changchun Huang[1]

[1]School of Geography, Nanjing Normal University, Nanjing, PR China, [2]Key Laboratory of Karst Dynamics, MNR & Guangxi, Institute of Karst Geology, Chinese Academy of Geological Sciences, Guilin, PR China, [3]Key Laboratory of Ecosystem Network Observation and Modeling, Institute of Geographic Sciences and Natural Resources Research, CAS, Beijing, PR China, [4]Taihu Laboratory for Lake Ecosystem Research, State Key Laboratory of Lake Science and Environment, Nanjing Institute of Geography and Limnology, Chinese Academy of Sciences, Nanjing, PR China

Abstract The boom in dam construction and continuous river-lake exchange has had a profound impact on the transmission and transformation of riverine dissolved inorganic carbon (DIC). An in-depth understanding of the change mechanisms of DIC concentrations and sources driven by dam operation and lake recharge is crucial for regulating greenhouse gas emissions and evaluating the impact of DIC on the global carbon cycle. This study investigated dam- and lakes-driven DIC via the concentration and $\delta^{13}C$ of DIC, combined with anions, cations, δD and $\delta^{18}O$ in the main stream of the Yangtze River. DIC showed a decreasing trend from upper reach (2,262.31 ± 113.69 μmol kg^{-1}) to lower reach (1,771.61 ± 89.36 μmol kg^{-1}). Carbonate dissolution proportion (from 36.45% to 28.44%) and atmospheric CO_2 proportion (from 37.51% to 22.94%) of DIC decreased from upper reach to lower reach, whereas soil CO_2 proportion of DIC (from 26.01% to 48.63%) increased. The control of dam operation on DIC biogeochemical process was revealed from different time scales. From the perspective of short-term seasonal changes (from 2020 to 2021), the mineralization of organic matter in the dry season strengthened CO_2 degassing and calcite precipitation, reducing the DIC and increasing the proportion of soil CO_2. Meanwhile, longer periods of runoff retention provided sufficient time for water–rock reactions in the wet season and increased the DIC and carbonate dissolution source in the reservoir area. On a long-term scale (from 2009 to 2021), a decrease in pH driven by sediment mineralization contributed to an annual increase in DIC in the reservoir. The flow of lakes mixed into the mainstream was revealed by the enrichment of $\delta^{18}O$, and river-communicating recharge decreased the DIC and carbonate dissolution source. We show that dam operation and lake inflow change DIC concentrations and sources and therefore need to be considered in the transmission and transformation processes of DIC in the river-ocean continuum.

Key Points:

- Compared to the dry season, dam operation increased the riverine dissolved inorganic carbon (DIC), and lake recharge decreased the DIC in the wet season
- Water retention by the reservoir increased the carbonate dissolution proportion of riverine DIC, but lakes flow mixed into the river decreased it
- Sediment mineralization increased annual pCO_2 and DIC concentrations in the Three Gorges Reservoir

Supporting Information:

Supporting Information may be found in the online version of this article.

Correspondence to:

C. Huang,
huangchangchun_aaa@163.com

Citation:

Zhao, C., Wang, C., Li, J., Meng, L., Xue, J., Gao, Y., et al. (2023). Changes in dissolved inorganic carbon across Yangtze River regulated by dam and river-lake exchange. *Global Biogeochemical Cycles*, *37*, e2023GB007749. https://doi.org/10.1029/2023GB007749

Received 22 FEB 2023
Accepted 31 AUG 2023

Author Contributions:

Writing – original draft: Chu Zhao
Writing – review & editing: Chu Zhao

1. Introduction

Rivers are vinculums of material connections between the atmosphere, soil, and biosphere, which contribute to the export of terrestrial carbon into estuaries and oceans and play a significant role in the global carbon cycle (Aufdenkampe et al., 2011; Catalán et al., 2016; Mendonça et al., 2017). Dissolved inorganic carbon (DIC) is an integral part of the carbon pool and is affected by the processes of photosynthesis, organic matter decomposition, calcite precipitation and dissolution that occur in the river system. Thus, mass transport and transformation of DIC have profound impacts on the global carbon cycle (Gao et al., 2022; Isaji et al., 2017; Pu et al., 2017). The process of CO_2 evasion from rivers is an important transformation of riverine DIC (Akhand et al., 2021; Xu et al., 2019) because most rivers are supersaturated with CO_2 (Raymond et al., 2013). Previous studies have proposed that the export of carbon from terrestrial ecosystems to inland water reached 1.9 Pg carbon per year (PgC yr^{-1}), of which 0.43 PgC was transported from rivers to the ocean in the form of DIC, and 0.8 PgC was transformed to CO_2 then emitted from rivers to the atmosphere (Cole et al., 2007; Probst et al., 1994; van Hoek et al., 2021). During the past decade, export of carbon from terrestrial ecosystems to inland water increased to 5.1 PgC yr^{-1}. Anthropogenic activities and organic matter mineralization increase DIC by varying degrees in many large rivers, such as Yangtze River, Ob River, and Mississippi River, in which the DIC concentrations have increased by 28.82%, 51.43%, and 61.23%, respectively (Cai et al., 2015; Drake et al., 2018; Gordeev et al., 1996; Hearth et al., 2022; Pipko et al., 2019; Voss et al., 2017; Zhang et al., 2014). Import of terrestrial carbon into rivers increased soil CO_2 proportion of DIC, thus CO_2 in most rivers becomes more supersaturated and contributes to global riverine CO_2 emissions, which have increased to 3.28 PgC yr^{-1} (Marx et al., 2017; Wen et al., 2021). Therefore, source

proportion and transformation processes of DIC have received increasing attention in geochemistry and with respect to the global carbon cycle (Campeau & Del Giorgio, 2014; Raymond & Hamilton, 2018).

Concerns regarding riverine DIC are primarily due to the substantial changes in its concentration caused by comprehensive natural and anthropogenic factors (Lu et al., 2022; Papadimitriou et al., 2005; Zhang et al., 2020). In natural water, HCO_3^- predominates DIC, which is partially regulated by the availability of weatherable minerals and the supply of weathering agents; thus, exogenous acids from agricultural and industrial production increase riverine DIC. Land leveling imports terrestrial materials into the river and promotes the contribution of organic matter mineralization to the increase in DIC. Dams intercept runoff and silt and regulate the riverine DIC's transport and transformation processes. The variation in riverine recharge will lead to an enrichment or dilution effect on DIC and may further affect the source proportion of DIC (Gao et al., 2020; Liu et al., 2016; Raymond & Hamilton, 2018; Song et al., 2020). Among these influential factors, the effect of damming and lake recharge on DIC has aroused widespread concern (Li, Pu, & Zhang, 2022; Wang et al., 2020). As over 16 million dams have been operating globally and many new dams will be built, biogeochemical processes of riverine DIC have significantly changed (Maavara et al., 2017). Heterotrophic microorganisms decompose terrestrial matter intercepted by dams to increase DIC and CO_2 proportion. CO_2 supersaturation results in outgassing and calcite precipitation to remove CO_2, then calcite precipitates and forms the inorganic carbon sink of the sediment (Gao et al., 2021; Zeng et al., 2019; Zhong et al., 2021a). Dams prolong the runoff retention period, reduce flow, strengthen water-rock interactions, and contribute to an increase in DIC concentration and carbonate dissolution. On the other hand, the flow of river-communicating lakes mixed into mainstream may directly change the DIC concentration and its source proportion because of different ion concentrations and rock weathering between lakes and rivers (Guo et al., 2023; Zhang et al., 2014). However, some knowledge gaps still exist regarding DIC transmission and conversion processes affected by damming and lake recharge. The seasonal variation in DIC production and consumption in reservoirs and the feedback mechanism of the response of the carbonate balance system to the continuous saturation of CO_2 in water remain unclear against the background of continuous exogenous carbon input. In monsoon regions, seasonal differences in the influence of lake recharge on riverine DIC require further evaluation. Carbon, deuterium, and oxygen isotopes will undergo fractionation due to differences in water retention time and supply sources; thus, isotope tracer technology can be used to investigate the effective mechanism of dam operation and lake recharge on DIC sources (Leybourne et al., 2006; Reyes-Macaya et al., 2022).

Riverine DIC originate from potential sources such as atmospheric CO_2, carbonate dissolution, and soil CO_2 (Chen et al., 2021; Song et al., 2020). The weathering of carbonate and silicate rocks consumes atmospheric CO_2 to produce DIC (Abongwa & Atekwana, 2015; Chetelat et al., 2008). Half of the carbon produced by carbonate weathering comes from atmospheric CO_2, and the other half comes from self-dissolution (Gao et al., 2020; Herath et al., 2020). Biogenic DIC originates from soil CO_2 produced by organic mineralization and CO_2(aqueous) formed by soil CO_2 dissolved in a solution (Cai et al., 2015; Telmer & Veizer, 1999). Due to the differences in activities between light (^{12}C) and heavy carbon isotopes (^{13}C), carbon isotopes of DIC ($\delta^{13}C_{DIC}$) undergo a series of physical, chemical, and biological reaction processes that result in different degrees of fractionation. For example, soil organic matter mineralization causes $\delta^{13}C_{DIC}$ to be influenced by the carbon isotope characteristics of terrestrial plants, thus causing $\delta^{13}C_{DIC}$ depletion, while atmospheric CO_2 weathering and carbonate dissolution cause $\delta^{13}C_{DIC}$ to become relatively enriched (Cotovicz et al., 2019; Samanta et al., 2015). Therefore, the proportion of DIC sources resulting from different reactions can be accurately reflected by variations in the $\delta^{13}C_{DIC}$ values. DIC formed by carbonate dissolution typically has a $\delta^{13}C_{DIC}$ value of −4.2‰ to −3.6‰ and an average of −3.9‰ (Ishikawa et al., 2015). DIC originating from rock weathering consumes atmospheric CO_2 with a $\delta^{13}C_{DIC}$ of approximately −2.5‰ (range −4.5‰ to −0.5‰) (Ishikawa et al., 2015; Shan et al., 2021). Soil CO_2 is formed by organic matter decomposition, and its $\delta^{13}C_{DIC}$ value (from −20.5‰ to −18.5‰, average −19.5‰) is affected by the overlying vegetation type (Telmer & Veizer, 1999). The $\delta^{13}C_{DIC}$ value of soil CO_2 dissolved in soil solution varies from −23‰ to −13‰ with an average of −17‰ (Amiotte-Suchet et al., 1999; Telmer & Veizer, 1999). As a result, additional isotope analysis of DIC may improve our understanding of the seasonal and spatial changes in DIC and the associated control mechanisms.

In the current study, we focused on the main stream of the Yangtze River to elucidate the effects of lake recharge and operation of the Three Gorges Dam (TGD) on DIC concentration and source. We adopted methods of DIC dynamic analysis, isotope tracer technology, and redundancy analysis to: (a) clarify the spatiotemporal distribution characteristics of DIC and sources in the main stream of the Yangtze River; (b) assess synchronous changes

in DIC concentration and sources disturbed by reservoir effect and river-communicating lakes recharge; and (c) reveal the environmental factors that affect the concentration and source of DIC.

2. Material and Methods

2.1. Study Area and Sampling

The Yangtze River originates from the Qinghai-Tibet Plateau and flows into the East Sea of China, with a main stream length of 6,400 km covering an area of 1.8×10^6 km^2 (Wang et al., 2008). The rock formation of the Yangtze River is mainly composed of Precambrian–Quaternary alluvium, evaporites, and carbonates (Zhao et al., 2022). Carbonate rocks are widely spread over the entire basin, particularly in the upper part of the main stream (Figure S1 in Supporting Information S1). The Dongting and Poyang Lakes are two river-communicating lakes mainly composed of sedimentary and metamorphic rocks located 1,400 and 800 km from the estuary, respectively (Zhang et al., 2014). The Yangtze River Basin is subject to a subtropical monsoon climate, alternately controlled by the Siberian winter and East Asian summer monsoon. The mean annual precipitation in the watershed is ∼1,142 mm. Precipitation during the wet season (May–October) accounts for 70%–90% of the total yearly rainfall (Wu et al., 2022; Zhang et al., 2014). Precipitation patterns during the two periods in this study showed significant differences; the monthly mean precipitation in December 2020 (14.1 mm) was lower than that in May 2021 (123.8 mm) (Figures S2a and S2b in Supporting Information S1). In main stream of the Yangtze River, monthly average discharge observed by hydrological stations in May (2.07×10^{10} m^3 S^{-1}) is significantly higher than that in December (4.55×10^{10} m^3 S^{-1}) (Figure S2c in Supporting Information S1). Therefore, December is considered as dry season and May is wet season in this study.

The TGD is located in the upper reaches of the Yangtze River, which extends from 1,850 to 2,300 km from the estuary of the East China Sea. The upstream of the TGR is more than 2,300 km away from the estuary, and the downstream of the TGD is 1,400–1,850 km away from the estuary. The operation state of the TGD can be divided into three stages: the construction stage (1994–2003), initial operation stage (2003–2008), and normal operation stage (after 2008) (Deng et al., 2016; Yang et al., 2014). In this process, the capacity and water regulation effect of the reservoir were enhanced, and its regulatory impact on the hydrology of the main stream was gradually highlighted. The maximum water level and storage capacity can reach 175 m and 39.3 km^3, respectively (Guo et al., 2021).

During the cruise from Chongqing to Shanghai along the main stream of the Yangtze River, 164 surface water samples were collected in December 2020 (62 samples collected within 14 days) and May 2021 (102 samples collected within 28 days) using a 10 L Niskin bottle (Figure 1). Subsequently, all water samples were filtered through 0.7 μm pre-combusted (450°C for 6 hr) Whatman quartz fiber filters. The filtrate was stored into precleaned high-density polyethylene (HDPE) bottles and stored in the dark at 4°C, then samples were transported to laboratory immediately.

2.2. Sampling and Laboratory Analyses

2.2.1. Chemical Analysis of Water Samples

The total dissolved carbon (TDC), dissolved organic carbon (DOC) in water were measured using a carbon elemental analyzer (Shimadzu Corporation., Japan) (Huang et al., 2018). Total suspended particulate matter (TSM) was measured by filtration with suspended particles dried at 55°C for 8 hr (Zhao et al., 2021). The IC-free TSS and filtrate were also used to measure particulate organic carbon (POC) using a carbon elemental analyzer (Huang et al., 2022). A multi-parameter meter (YSI ProDss., USA) was used to analyze the water pH (scale is 0–14), dissolved oxygen (DO), specific conductivity (Spc), turbidity, and water temperature (Tw) for field measurements. Chlorophyll-*a* (Chl *a*) and total nitrogen (TN) levels were determined using a UV-3600 spectrophotometer (Shimadzu Corp., Japan) (Huang et al., 2017). Major anions and cations (Ca^{2+}, Mg^{2+}, SO_4^{2-}, Na^+) were measured using Dionex ICS-900 ion chromatography (Dionex, USA) based on the APHA 2012 method (Rice et al., 2012). Acid neutralizing capacity (ANC) was calculated by anions and cations. Saturation index of calcite (SIc) was calculated by the software of PHREEQC Interactive 3.6.2 (Text S1 in Supporting Information S1). δD and $\delta^{18}O$ were measured using a mouse FAT/LEAN imaging analyzer (Picarro, USA) at the Chinese Academy of Geological Sciences (Guangxi, China) (Wu et al., 2022), and deuterium excess (d-excess) was calculated using the formula: d-excess = $\delta D - 8\delta^{18}O$ (Craig, 1961).

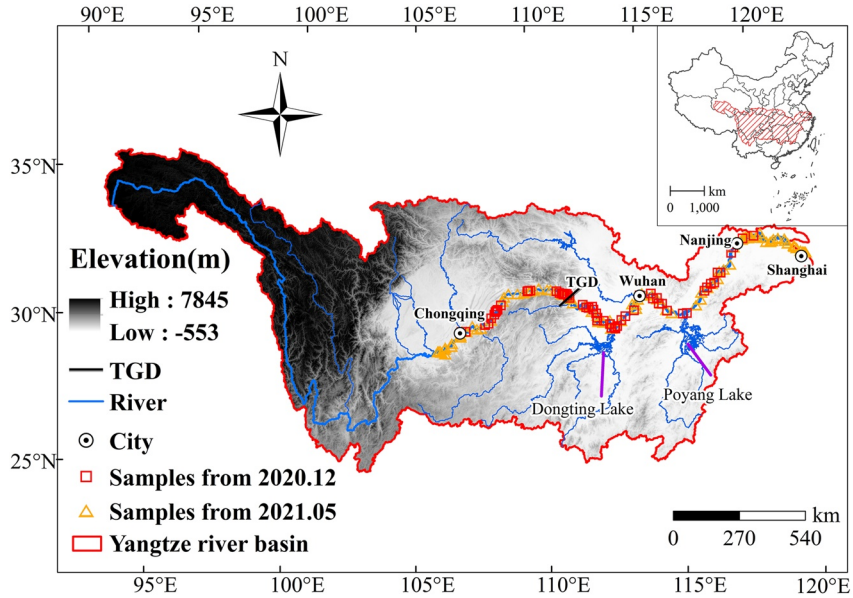

Figure 1. Study area and sampling sites. The red squares and orange triangles represent water samples collected in December 2020 and May 2021, respectively. The location of TGD is shown in the figure, together with the metropolitan cities Chongqing, Wuhan, Nanjing, and Shanghai.

2.2.2. Measurement of DIC Concentration and Its Stable Carbon Isotope

DIC concentration were measured using TOC-L analyzer (Shimadzu Corporation., Japan) equipped with an ASI-Lsampler in total inorganic carbon (IC) mode (Gu et al., 2020; Wang et al., 2016). We pretreated water samples using glass fiber filters (Whatman quartz fiber filters, 0.7 μm) to avoid interference caused by PIC (particulate inorganic carbon, mean value of 22.09 μmol kg^{-1}, Text S2 and Figure S3 in Supporting Information S1) on the DIC and carbon isotope analysis. To evaluate the influence of air-water exchange on the precision and accuracy of DIC during filtration process, we used CO_2SYS software to calculate DIC through total alkalinity (TA), Tw and pH (Pierrot et al., 2006). The TA was determined by unfiltered water in the field using hydrochloric acid (HCL) titration with a Titrette Digital Titrator (Brand Trading Co., Ltd, Wertheim, Germany), HCL titrant was 0.05 mmol L^{-1} (Zhang et al., 2019). The comparison result showed precision error between measured and calculation value was 5.73% (in December) and 4.77% (in May) (Figure S4 in Supporting Information S1), we used measured DIC by TOC-L analyzer in this study. Isotopes of DIC ($\delta^{13}C_{DIC}$) were determined using Thermo MAT253 plus (Thermo Fisher Scientific, Germany) with a Gas Bench II automated device (Thermo Fisher Scientific, Germany) (Su et al., 2019). The carbon isotope ratios of DIC were expressed in delta notation ($\delta^{13}C$) relative to Vienna PDB, and the standard deviations based on replicate measurements for $\delta^{13}C$ were ~0.05‰ (Li, Pu, & Zhang, 2022).

2.3. Model Application

2.3.1. Bayesian Mixing Model

DIC source analysis by a Bayesian mixing model was conducted using the "MixSIAR" package in R 4.0.4 software, which is based on the Dirichlet distribution and the logical prior distribution of the Bayesian framework (Duvert et al., 2020; Evans et al., 2000). The Bayesian mixing model improves on the simpler linear hybrid model by explicitly considering uncertainty in source values, categories, and continuous covariates (more described in Text S3 of the Supporting Information S1). Previous experiments illustrated that $\delta^{13}C_{DIC}$ does not exhibit significant changes in 10 hr (Abongwa & Atekwana, 2018). However, numerous reservoirs in the main stream of the Yangtze River contribute to the difference in the hydraulic retention time in stream segments, which leads to significant challenges and uncertainty in the calculation of DIC isotope fractionation caused by the water-atmosphere exchange in the large river. Accordingly, the DIC in the main stream of the Yangtze River was considered to be in chemical equilibrium with degassed CO_2. Bayesian mixing models were not involved

in isotope fractionation caused by water-atmosphere CO_2 interaction (Shan et al., 2021; Song et al., 2021). Data from the $\delta^{13}C_{DIC}$ were categorized based on each month's upper, middle, and lower reaches to calculate the source component. The range of DIC sources was statistically estimated using end-member values from previous studies (Table S1 in Supporting Information S1). In addition, the $\delta^{18}O$ values of the main stream before lake recharge and of the lake (Table S3 in Supporting Information S1) were viewed as two end members, based on the variation of $\delta^{18}O$ after lake recharge into the main stream, and were to calculate the contribution of the lake water supply to the main stream of the Yangtze River.

2.3.2. Structural Equation Modeling

Structural equation modeling (SEM) was used to test and quantify the impact of environmental factors (temperature and pH that affect carbonate equilibrium system) and dam behavior on the DIC transformation process in the reservoir area. SEM is an advanced generalized linear regression model, which evaluates the effectiveness of covariance matrix by computing multiple relationships between variable related to DIC transformation (Amini & Alimohammadlou, 2021). The model can not only examine the direct influence among variables but also reveal the indirect influence among variables. Important parameters involved in the model are goodness of fit index (GFI) and comparative fit index (CFI), which should be more than 0.90. Root mean square error of approximation (RMSEA) should be less than 0.10 to illustrate reasonable and reliable network (Nakayama et al., 2022). In this study, GFI and CFI of the model are more than 0.95, RMSEA is less than 0.05; thus, the credibility of the model has been verified. The models were designed using the software of AMOS 25.0.

2.4. Data Sources Collected From Published Data

To assess long-term variation of DIC concentration affected by TGR and lakes, historical data sets including discharge, sediment loads, water quality parameters, δD, $\delta^{18}O$, pCO_2, concentrations of riverine nutrients and elements were gathered. Discharge and sediment records were collected from previous study (Zhang et al., 2014) and the Yangtze Sediment Bulletin (http://www.cjw.gov.cn/), respectively. Water quality parameters δD, $\delta^{18}O$, pCO_2, nutrients, and major ions were extracted from published sources given in Tables S3–S6 of the Supporting Information S1.

2.5. Processes Affecting DIC Concentrations and $\delta^{13}C_{DIC}$

The variation in the DIC concentration and $\delta^{13}C_{DIC}$ in most reservoirs is often caused by a mixture of biogeochemical and physical processes, which include (a) CO_2 exchange across the air-water interface, (b) photosynthesis dominated by phytoplankton, (c) degradation of organic matter, and (d) dissolution or precipitation of calcite (Samanta et al., 2015; Su et al., 2019). To reveal the relevant processes and driving factors of DIC migration and transformation, water in the upstream of TGR was used as the reference value to evaluate DIC transformation processes in the reservoir and downstream. The changing degree of DIC and $\delta^{13}C_{DIC}$ was calculated by following equations (Wang et al., 2019, 2020):

$$\Delta\left[\delta^{13}C_{DIC}\right] = \delta^{13}C_{DIC}(\text{in reservoir or downstream}) - \delta^{13}C_{DIC}(\text{upstream}) \quad (1)$$

$$\Delta\,[DIC] = [DIC](\text{in reservoir or downstream}) - [DIC](\text{upstream}) \quad (2)$$

3. Results

3.1. Decreasing Trend of DIC From the Upper to Lower Reaches

The concentration of DIC varied from 1,632.58 to 2,448.50 μmol kg^{-1} with mean value of 2,049.48 ± 242.50 μmol kg^{-1}, which displayed a gradually decreasing trend from the upper to lower reaches. DIC presented a linear relationship with the distance from the estuary (y defined as DIC and x is distance of samples from estuary, then $y = 0.27x + 1{,}729.61$, $R^2 = 0.76$) (Figure 2a). The seasonal difference in DIC in the main stream of the Yangtze River was significant (Table S2 in Supporting Information S1), the highest DIC was observed in December (mean value of 2,092.06 ± 126.05 μmol kg^{-1}), followed by in May (2,023.61 ± 289.00 μmol kg^{-1}) (Figure 2a). In addition, the DIC in May showed a higher spatial change rate (linear regression slope with samples distance

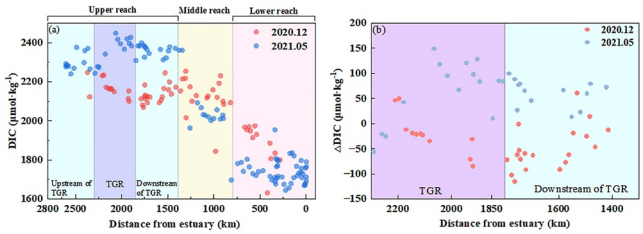

Figure 2. (a) Spatiotemporal variation of DIC exhibiting decrease trend from upper to lower reach of the Yangtze River. Note that the main stream was separated into upper (blue background), middle (yellow background), and lower reach (red background), the extent of TGR was highlighted by purple background; the fitting line between distance (from estuary to upper reach) and DIC during two periods was $y = 0.27x + 1{,}729.61$, $R^2 = 0.76$; the fitting line in December 2020 was $y = 0.15x + 1{,}882.83$, $R^2 = 0.49$ and the fitting line in May 2021 was $y = 0.30x + 1{,}698.32$, $R^2 = 0.83$. (b) The difference of Δ [DIC] between samples in TGR and downstream of TGR.

from estuary, slope = 0.30) and spatial variation (coefficient of variation, CV = 0.14) than those in December (slope = 0.15, CV = 0.06).

Cluster analysis of DIC suggested that the main stream of the Yangtze River can be separated into three reaches (upper, middle, and lower) (Figure S5 in Supporting Information S1), and the boundaries were found at 1,400 km (located near the Dongting Lake) and 800 km (located near the Poyang Lake) away from the estuary. DIC showed significant differences between each reach ($p < 0.05$) (Figure 2a; Table S2 in Supporting Information S1), which in the upper reach (averaged 2,257.02 ± 110.39 μmol kg^{-1}) was 8.06% and 27.70% higher than that in the middle reach and lower reach, respectively. In December, DIC decreased slightly from upper reach to middle reach, contributing to its higher value compared to the samples in May in middle reach (Figure 2a; Table S2 in Supporting Information S1). In addition, the mean value of the DIC in TGR was lower than its upstream in December, but the opposite variation of DIC was observed in May. The DIC in the TGR was higher than that in its downstream. Notably, the mean value of the DIC in TGR in May was 201.34 μmol kg^{-1} higher than that in December, and this seasonal concentration difference was further increased to 225.42 μmol kg^{-1} in its downstream. Positive Δ[DIC] values occurred mostly in May, indicating that the DIC was higher in the reservoir and downstream of the TGR than upstream (Figure 2b). However, this phenomenon was seasonal, and negative Δ[DIC] values occurred mostly in December, indicating that the DIC concentration upstream of the reservoir was higher.

3.2. Characteristics of Carbon Isotope and Source of DIC

The $\delta^{13}C_{DIC}$ value exhibited a decreasing trend from upper reach (−7.46 ± 0.52‰) to lower reach (−9.15 ± 0.41‰). The $\delta^{13}C_{DIC}$ values between each reach showed significant differences ($p < 0.05$), where values were more enriched in the upper reach and close to the characteristic value of carbonate dissolution (−3.9 ± 0.3‰), then depleted from the middle to lower reaches and close to the characteristic value of soil CO_2 (−17 ± 4.0‰) (Figure 3a; Table S2 in Supporting Information S1). The value of $\delta^{13}C_{DIC}$ exhibited significant seasonality during these two periods (Figure 3a). $\delta^{13}C_{DIC}$ in May was highly depleted (−8.57 ± 0.89‰) and close to the characteristic value of soil CO_2 (Figure 3a; Table S2 in Supporting Information S1). In contrast, $\delta^{13}C_{DIC}$ was highly enriched in December (−7.85 ± 0.78‰) and close to the characteristic value of carbonate dissolution. The values of $\delta^{13}C_{DIC}$ showed a depleted trend from the upstream of TGR to its downstream. The negative value of Δ [$\delta^{13}C_{DIC}$] occurs May, which means $\delta^{13}C_{DIC}$ was enriched upstream of TGR compared to the reservoir and downstream. Negative Δ[$\delta^{13}C_{DIC}$] values occurred in May, indicating that the $\delta^{13}C_{DIC}$ was enriched upstream of the TGR compared to in the reservoir and downstream. Notably, although negative Δ[$\delta^{13}C_{DIC}$] values occurred mostly in December, the $\delta^{13}C_{DIC}$ difference in these areas was smaller than that in May, and the $\delta^{13}C_{DIC}$ at some sample points in the reservoir and downstream of the TGR was even more enriched than that upstream (Figure 3b).

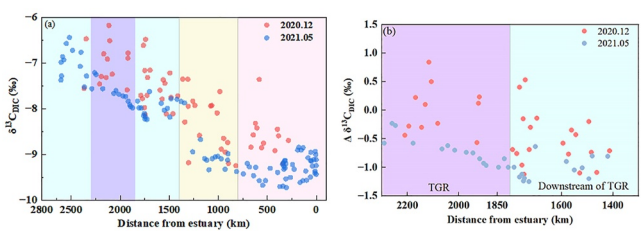

Figure 3. Spatiotemporal variations of $\delta^{13}C_{DIC}$ exhibiting depleted trend from upper to lower reach of the Yangtze River. Note that the result of fitting line between distance (from estuary to upper reach) and $\delta^{13}C_{DIC}$ during two periods was $y = 0.97 \times 10^{-3} \times -9.91$, $R^2 = 0.38$; the fitting line in December 2020 was $y = 1.02 \times 10^{-3} \times -9.50$, $R^2 = 0.87$ and the fitting line in May 2021 was $y = 0.96 \times 10^{-3} \times -9.59$, $R^2 = 0.85$. (b) The difference of Δ [$\delta^{13}C_{DIC}$] between samples in TGR and downstream of TGR. The blue, yellow, and red backgrounds indicated the range of upper, middle, and lower reach, respectively. The extent of TGR was highlighted by purple background.

The source estimation of $\delta^{13}C_{DIC}$ via the Bayesian mixture model exhibited well-defined spatial and seasonal characteristics in the main stream of the Yangtze River. The source proportion of carbonate dissolution and atmospheric CO_2 both showed a decreasing trend from upper reach to lower reach. In contrary, the source proportion of soil CO_2 increased from upper reach (26.01% ± 5.15%) to lower reach (48.63% ± 4.25%). The average contribution of carbonate dissolution to DIC was higher in December (34.48% ± 3.65%) than that in May (31.09% ± 4.82%), whereas the proportion of soil CO_2 components decreased from May (40.38% ± 11.77%) to December (29.34% ± 6.99%) (Figure 4). Atmospheric CO_2 proportion of DIC decreased from upper to middle reach in December, located near the basin of the Dongting Lake (Figure 4a). In May, the proportion of carbonate dissolution and atmospheric CO_2 to DIC smoothly decreased from the upper to lower reach, whereas the soil CO_2 proportion to DIC showed the opposite

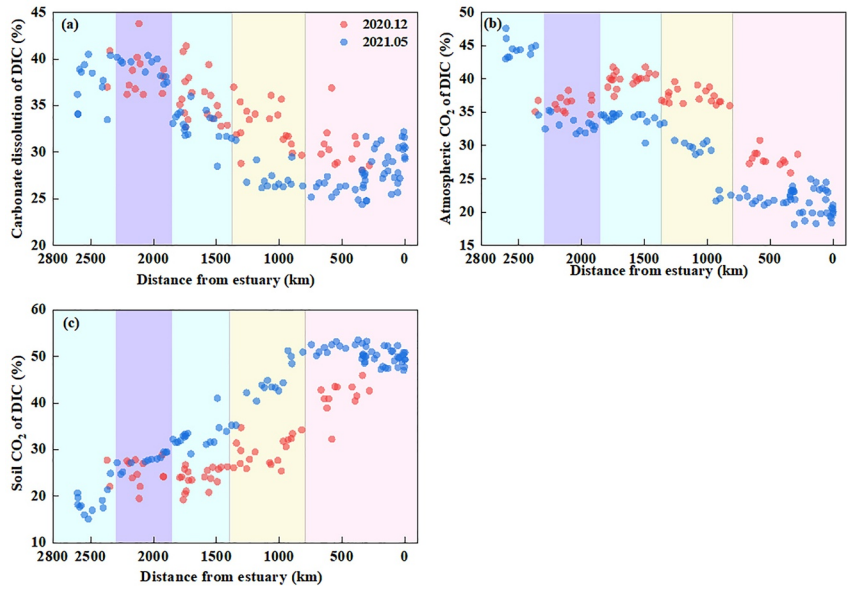

Figure 4. Spatiotemporal variation of the contribution proportion of the DIC source. (a) Carbonate dissolution, (b) atmosphere CO_2, and (c) soil CO_2. The blue, yellow, and red backgrounds indicated the range of upper, middle, and lower reach, respectively. The extent of TGR was highlighted by purple background.

trend. The contribution of soil CO_2 to DIC increased from the upstream of TGR to its downstream. In addition, the proportion of carbonate dissolution to DIC in December decreased along the upper reaches of the Yangtze River. However, the source of carbonate dissolution in TGR was significantly higher than that in the downstream of TGD in May. The soil CO_2 proportion of DIC in TGR was higher than that in its upstream and downstream in December.

3.3. Hydrological Signals From Upper to Lower Reach

$\delta^{18}O$ and δD in the main stream water exhibited synchronous enrichment from the upper to lower reach during the study period. The values of $\delta^{18}O$ and δD between each reach showed significant differences ($p < 0.05$) (Table S2 in Supporting Information S1), such that $\delta^{18}O$ in the upper reach ($-11.13 \pm 0.75‰$) was more depleted than that in the middle reach ($-9.22 \pm 1.10‰$) and lower reach ($-7.53 \pm 0.59‰$) (Figure 5a). Notably, $\delta^{18}O$ and

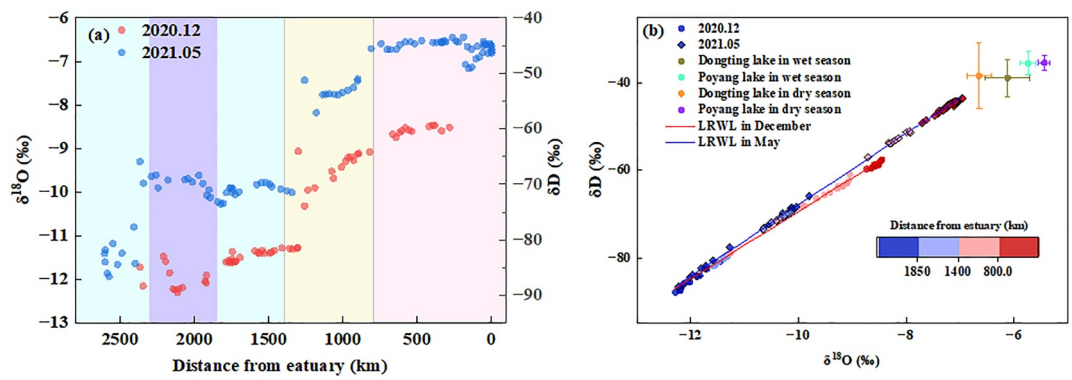

Figure 5. (a) Spatiotemporal variations of $\delta^{18}O$ and δD exhibiting enriched trend from upper to lower reach of the Yangtze River. The blue, yellow, and red backgrounds indicated the range of upper, middle, and lower reach, respectively. The extent of TGR was highlighted by purple background. (b) Local runoff water line (LRWL) of the Yangtze River. $\delta^{18}O$ and δD in lakes showed more enriched than that in lakes. Red fitting line between δD and $\delta^{18}O$ is data in December 2020 ($\delta D = 7.70\delta^{18}O + 7.59$, $R^2 = 0.99$); the blue fitting line is data in May 2021 ($\delta D = 8.17\delta^{18}O + 13.83$, $R^2 = 0.99$). The detailed historical data of $\delta^{18}O$ and δD in two lakes in Table S3 of the Supporting Information S1.

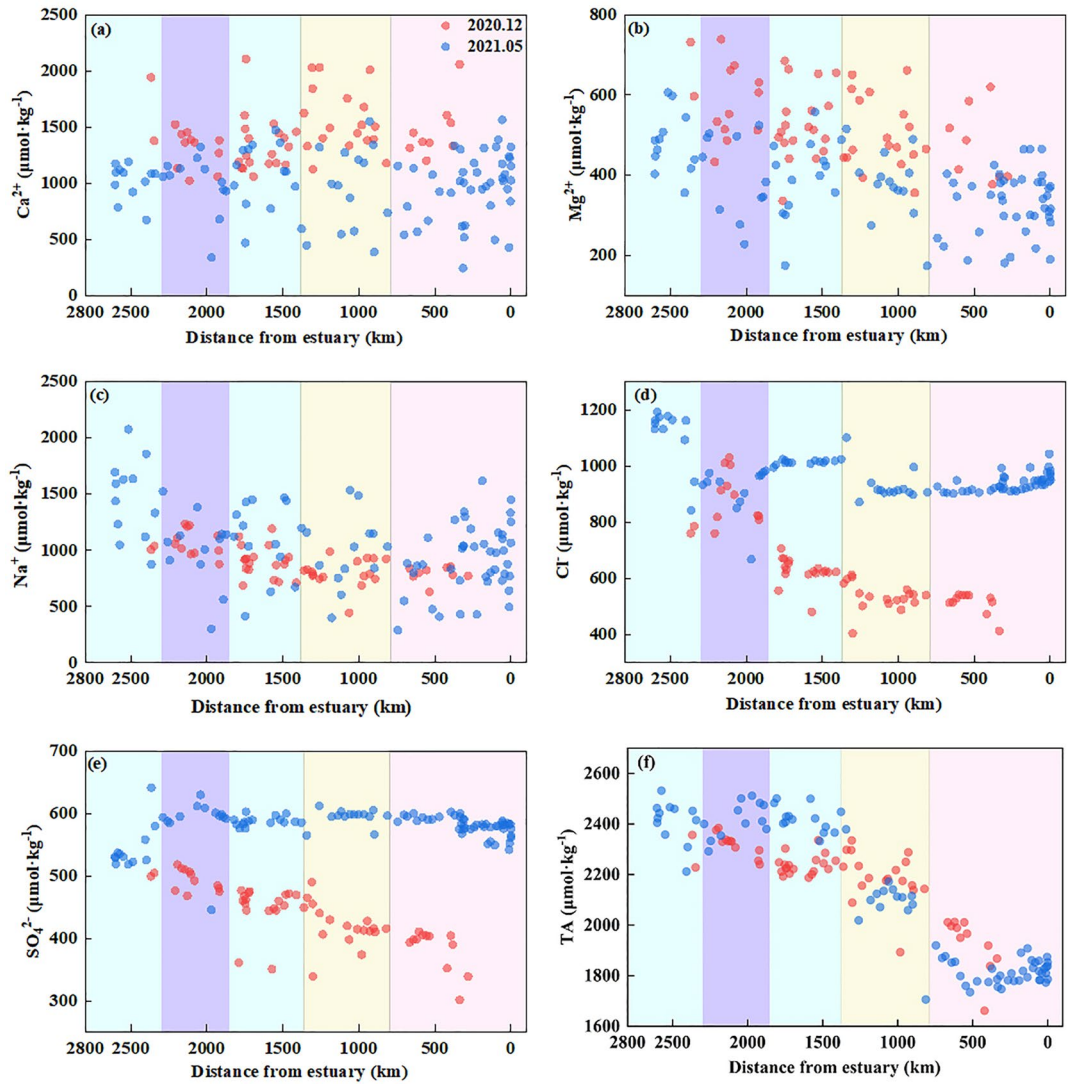

Figure 6. Spatiotemporal distribution of major cations and anions in the main stream of the Yangtze River. (a) Ca^{2+}; (b) Mg^{2+}; (c) Na^{2+}; (d) Cl^{-}; (e) SO_4^{2-}; (f) TA. The blue, yellow, and red backgrounds indicated the range of upper, middle, and lower reach, respectively. The extent of TGR was highlighted by purple background.

δD in Dongting Lake and Poyang Lake were more enriched than that in the main stream of the Yangtze River during two seasons (Figure 5b). Local runoff water line (LRWL, linear regression of δD and $\delta^{18}O$) in the main stream of the Yangtze River showed pronounced seasonality. A higher spatial variation in LRWL was observed in May (CV = 0.19), followed by in December (CV = 0.13). The average rate of change in $\delta^{18}O$ and δD in May (slope = 8.17) was higher than that in December (slope = 7.70). The variation range of $\delta^{18}O$ in the middle reach in May (−10.42–7.27‰) was greater than that in December (−11.30 to −9.06‰) (Figure 5b). The $\delta^{18}O$ increased significantly from the upstream of TGR (−11.55 ± 0.75‰) to the reservoir area (−10.25 ± 0.16‰). In addition, the LRWL during the two periods was close to the line of the global meteoric water line (GMWL) and the Meteoric Water Line of China, which indicated that water in the main stream of the Yangtze River was mainly from precipitation recharge (Figure S6 in Supporting Information S1).

3.4. Major Ion Compositions and TA in the Main Stream

The major cation and anion concentration values followed the order $Ca^{2+} > Na^{+} > Cl^{-} > Mg^{2+} > SO_4^{2-}$. The concentration of Ca^{2+} in December (1,439.79 ± 261.72 μmol kg^{-1}) was higher than that in May (1,006.49 ± 292.49 μmol kg^{-1}) (Figure 6a). The Mg^{2+} concentration range from 753.89 to 1,714.63 μmol kg^{-1}

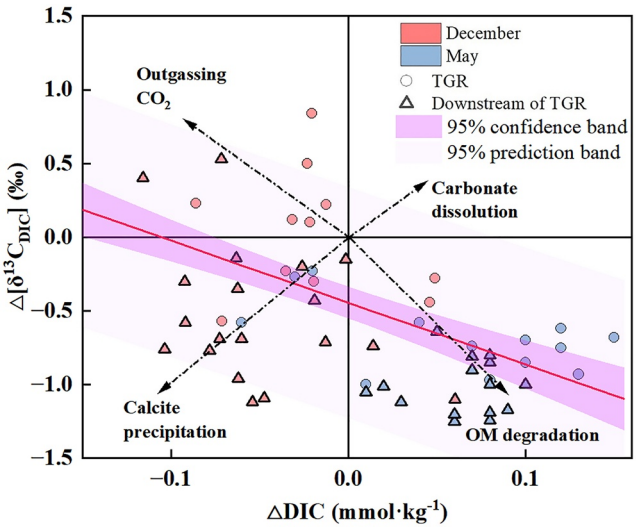

Figure 7. The relationship between Δ [DIC] and Δ [$\delta^{13}C_{DIC}$] for samples in TGR and its downstream. Note that circles represent samples in TGR and triangles represent samples in downstream of the reservoir area. Samples in different quadrants affected by corresponding process, such as outgassing CO_2, calcite precipitation, carbonate dissolution and organic matter degradation.

with mean value of 434.60 ± 124.23 μmol kg^{-1} in the main stream, which in December was 1.49 times higher than that in May (Figure 6b). Na^+ in December showed lower variability and concentration (893.29 ± 156.76 μmol kg^{-1}) than that in May (1,053.39 ± 237.18 μmol kg^{-1}) (Figure 6c). Cl^- decreased from the upper reach (894.00 ± 188.57 μmol kg^{-1}) to the lower reach (848.95 ± 181.19 μmol kg^{-1}) in the Yangtze River during the two periods, which reflects the decreasing contribution of evaporites from the upper reach to the lower reach (Figure 6d). SO_4^{2-} in December decreased from the middle to lower reach, and in May, it varied smoothly in the entire basin with a mean of 581.935 ± 23.44 μmol kg^{-1} (Figure 6e).

The TA values were significantly different ($p < 0.05$) in the three reaches during the sampling periods. TA values were high in the upper reaches (2,351.31 ± 96.53 μmol kg^{-1}), then decreased from the middle reaches (2,158.22 ± 134.55 μmol kg^{-1}) to the lower reaches (1,842.60 ± 77.66 μmol kg^{-1}) (Figure 6f). The mean value of TA in December was 2,179.36 ± 154.26 μmol kg^{-1} and reached a lower value in May (2,115.14 ± 287.66 μmol kg^{-1}) (Figure 6f). The temporal and spatial variation trend of alkalinity was consistent with DIC, which indicated that the biogeochemical processes of DIC and TA were regulated by TGR and two large lakes (Figures 2 and 6f).

4. Discussion

4.1. Dam Operation Constrains Riverine DIC Concentration and Source

4.1.1. Outgassing CO_2 and Calcite Precipitation Process in Dry Season

The outgassing of CO_2 and calcite precipitation were the main factors affecting the lower DIC concentrations in the reservoir and its downstream area in December (Figure 7). The flux of sediments reached 1.07×10^6 t yr^{-1} in the TGR (Li et al., 2021). Interception of terrestrial and autochthonous organic matter by dams regulated the DIC cycle. With the reduction in phytoplankton photosynthesis in December, mineralization of resuspended sedimentary organic matter further yielded CO_2 to reduce the pH and DO of surface water in TGR (Liu et al., 2016) (Figures S7c and S7e in Supporting Information S1). This process increased the soil CO_2 proportion of DIC in the reservoir area. The pCO_2 in the reservoir decreased from depth of 18 m to surface water in December, further indicating the process of escaping the accumulated CO_2 from reservoir bottom to the surface (Figure S8a in Supporting Information S1). Increased CO_2 emissions from degassing cause DIC consumption in the reservoir area (Li et al., 2018). Notably, pCO_2 downstream of TGR increased from the depth to the surface, and its value was lower than that in the reservoir (Figure S9 in Supporting Information S1). The similar water column temperatures indicated that temperature was not the main reason for the difference of pCO_2 (17.50 and 17.66°C). This phenomenon may have been caused by the reduction in sediment because POC and DOC concentrations decreased from the deep water to surface water downstream of the dam (Figures S8b and S8c in Supporting Information S1). The reduction of organic matter weakens the mineralization downstream of TGR. Higher pH and lower pCO_2 facilitated calcite precipitation (Equation 3). The significant correlation between $\Delta[Ca^{2+}]$ and Δ[DIC] downstream of TGR ($r^2 = 0.44$) in December reveals that the DIC decreased due to calcite precipitation (Figure S10 in Supporting Information S1).

$$Ca^{2+} + HCO_3^- \leftrightarrow CaCO_3\downarrow + H_2O + CO_2\uparrow \quad (3)$$

4.1.2. Organic Matter Degradation and Retention Effect in Wet Season

Abundant precipitation in the wet season led to a continuous flow of terrestrial organic matter into the TGR. The degradation of organic matter increased the soil CO_2 proportion of DIC and contributed to depleting the $\delta^{13}C_{DIC}$ (Figure 7). Although the degradation of organic matter may increase dissolved CO_2 in water, the negative correlation between Chl *a* and dissolved CO_2 ($r = -0.49$, $p < 0.01$) in the reservoir area in May highlighted how CO_2 outgassing was weakened by phytoplankton photosynthesis (Figure S11 in Supporting Information S1) (Pu

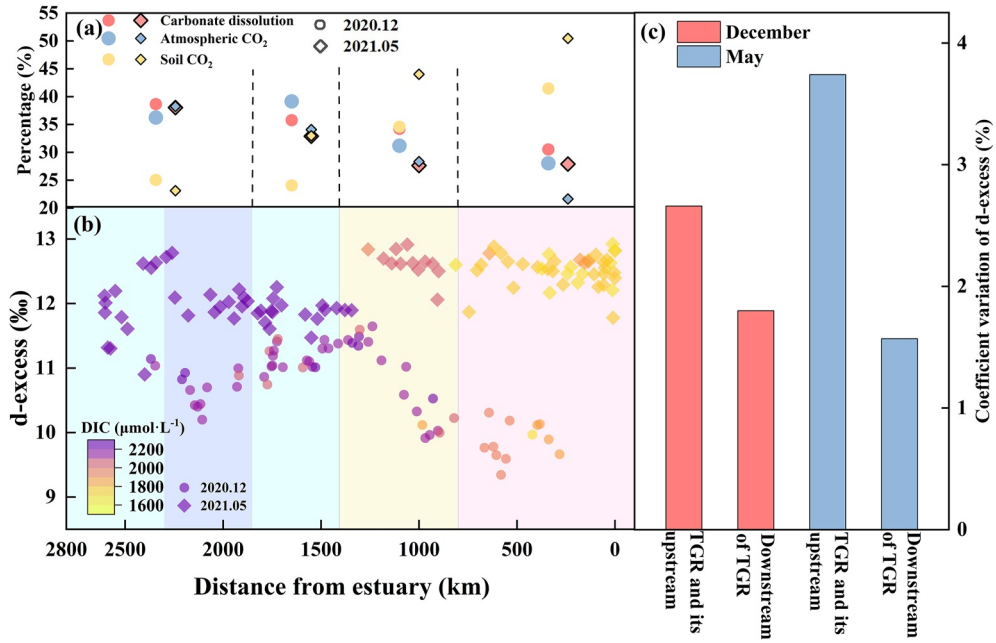

Figure 8. (a) DIC source proportion in different reaches; (b) The value of d-excess in the main stream of the Yangtze River; (c) Coefficient variation d-excess of TGD and its upstream versus downstream. According to the geographical location, purple boxes are used to identify the extent of the reservoir area and distinguish its upstream and downstream. Blue, yellow and red shaded areas indicate upper, middle, and lower reaches in this study, respectively.

et al., 2017; Uthicke & Fabricius, 2012). In addition, dam impoundment increased the DIC and its carbonate dissolution proportion in May (Figure 8a). Longer residence time of water in reservoirs induced more vigorous mixing, contributing to relatively smaller fluctuations in the isotopic signatures and manifesting as lower CV of d-excess (Figure 8b) (Deng et al., 2016; Wu et al., 2022). Based on the monthly storage change and outbound flow, the assessment results indicated that the drainage period of the reservoir in May was 3.38 times longer than that in December (Text S5 in Supporting Information S1). Longer retention time contributed to the lower CV of d-excess in May (1.5%) than that in December (1.7%) (Figure 8c). The extended period of water retention in the reservoir in May decreased the runoff flow. The sufficient time for water–rock reactions to occur due to the extended retention time increased the carbonate dissolution proportion and DIC concentration in the TGD and its upstream area in May (Figures 2a and 3a) (Han et al., 2018; Wu & Firoozabadi, 2010).

SEM revealed the feedback mechanism of the carbonate balance system to continuous saturation of CO_2 driven by sediment mineralization in the reservoir water from 2009 to 2021 (TGD in the normal stage). Mineralization of the accumulated sediment yields saturated pCO_2 in the reservoir water, thereby promoting calcite precipitation and reducing the acid neutralization capacity of water (Figure S12 in Supporting Information S1). The carbonate buffer system alleviated the decrease of pH by enhancing the outgassing of CO_2, which further formed a positive feedback loop of water acidification in the reservoir area (Figure 9a). Previous studies indicated that more acidified conditions would promote carbonate dissolution and result in an increase in TA and HCO_3^- (Kapetanaki et al., 2018, 2020). Notably, the SEM results show that pCO_2 variation has no significant impact on DIC concentration ($p > 0.05$), which can be attributed to the interannual variation of DIC in TGD driven by HCO_3^- generated by mineralization and water acidification, rather than the loss of DIC caused by CO_2 outgassing (Figures 9b and 9c). Thus, sediment mineralization increased annual pCO_2 and DIC concentrations in the TGR.

4.2. River-Communicating Lake Recharge Regulates DIC Concentrations and Sources

The significant negative correlation between DIC concentration and $\delta^{18}O$ only occurred downstream of Dongting and Poyang lake; thus, the flow of lakes mixed into main stream enriches hydrological signals and contributes to the dilution effect of DIC (Figure 10a). Wide surface area and slow runoff make water in lakes suffer intense sub-cloud secondary evaporation, thus more enriched deuterium and oxygen signal formed in lakes than that in main stream (Deng et al., 2016; Ding et al., 2014; Li, Song, et al., 2022). Isotopic source analysis (δD and

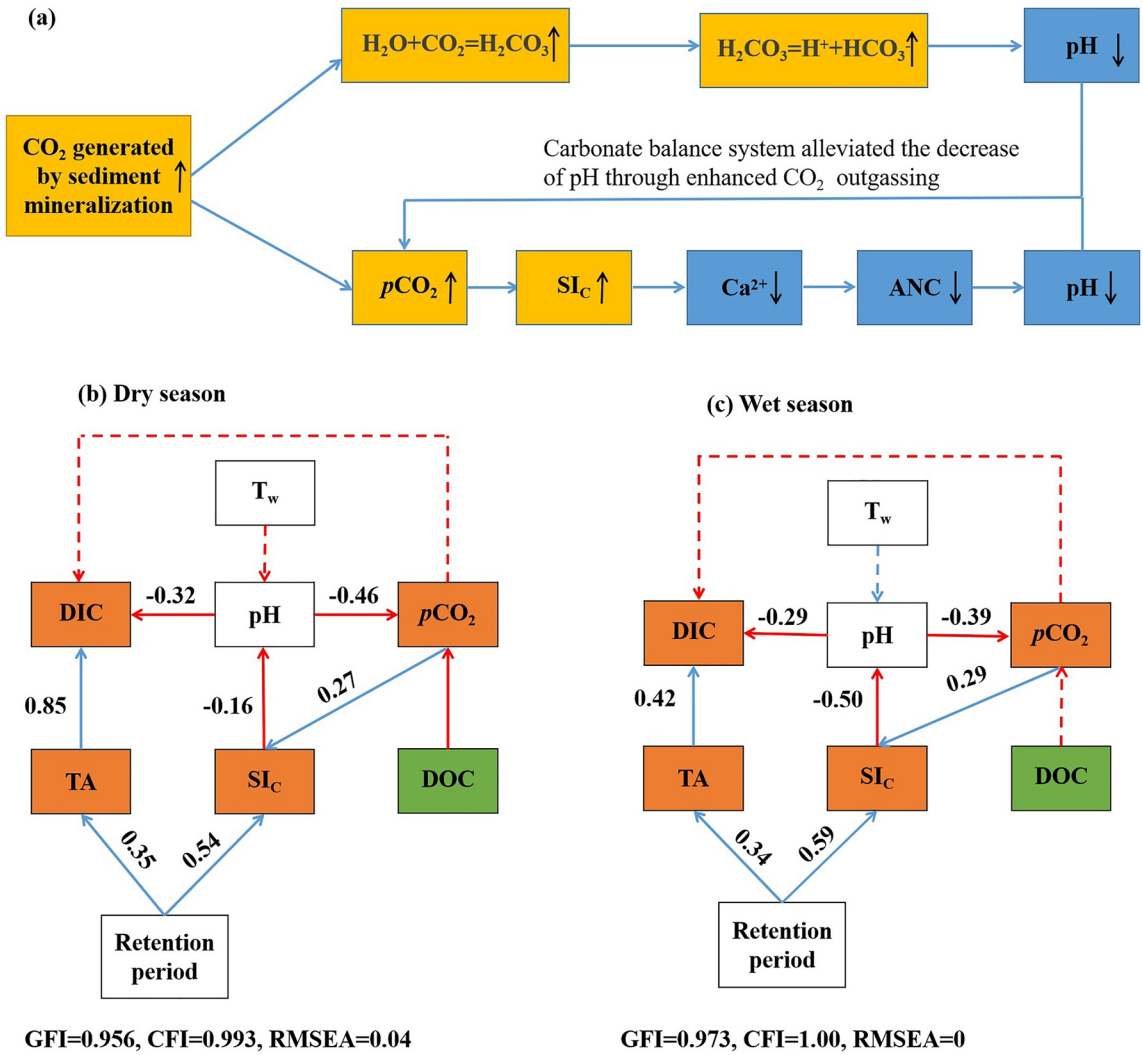

Figure 9. The impact of environmental factors on DIC in the reservoir area (a) feedback mechanism of carbonate balance system response to continuous saturation of CO_2, yellow boxes represent increasing trends and blue represent decreasing trends; (b) dry season; (c) wet season. In SEM model, blue and red solid lines indicate the significant positive and negative correlation paths ($p < 0.05$), solid and dashed lines suggest significant ($p < 0.05$) and not significant correlation ($p > 0.05$). Orange boxes represent inorganic system and the green represent organic carbon. Some of data were compiled from (Wu and Han (2018), Hearth et al. (2020), Li et al. (2020a, 2020b), detailed in Table S4 of the Supporting Information S1), and other data were collected from this study.

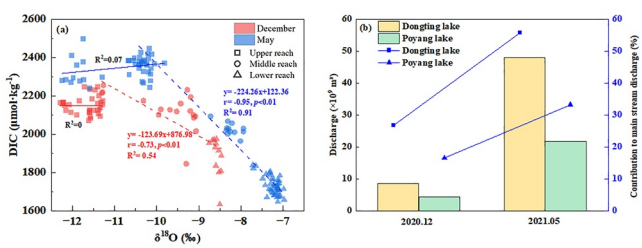

Figure 10. (a) Relationships between DIC and $\delta^{18}O$ during the two periods in the main stream of the Yangtze River, the squares, circles, and triangles symbols indicated the range of upper, middle, and lower reach, respectively; (b) Contribution proportion of lakes recharge to discharge of main stream, the contribution percentage is calculated using Bayesian mixing model and end member of $\delta^{18}O$ are samples near lakes-river confluence and historical value of two lakes in Figure 5b.

$\delta^{18}O$) showed that the contribution of Dongting Lake and Poyang Lake to the main stream discharge in December was 26.7% and 16.5%, compared with 55.7% and 33.1% in May. These results are consistent with the changes in lake discharge monitored by the hydrological stations (Figure 10b). Therefore, lake recharge was the main cause of the variation in the hydrological signals and DIC in the middle and lower reaches. The results of ion stoichiometry and carbon isotope analyses further explained the spatial variation in the DIC. Carbonate weathering by CO_2(aq) gradually weakened in the lake inflow area, which led to a decreasing trend in the DIC, carbonate dissolution, and atmospheric CO_2 proportions from the middle to lower reaches (Figure 8). Previous studies have revealed that carbonate weathering weakens from the middle to the lower reaches because of the lower abundance of carbonate rocks, which is consistent with the results of this study (Figure S1 in Supporting Information S1) (Zachara et al., 2016; Zhang et al., 2014). In

addition, river-communicating lakes are considered terrestrial carbon sinks that export terrigenous substances to increase the soil CO_2 proportion of DIC (Cao et al., 2016; Lu et al., 2018).

Seasonal differences in the DIC concentration and source proportion in the middle and lower reaches are regulated by lake recharge in the Yangtze River (Chetelat et al., 2008; Shan et al., 2021). The higher contribution of lake recharge to the main stream and the better fitting relationship between the DIC and $\delta^{18}O$ ($R^2 = 0.91$) indicated that the DIC was more influenced by lake contributions to discharge in May than in December (Figures 10a and 10b). Lakes recharge diluted the TA and reduced the contribution of carbonate dissolution to DIC, which result in lower DIC in the middle and lower reaches in May (Figures 4a and 6f). Notably, the concentrations of Ca^{2+} and Mg^{2+} in the middle and lower reaches in December were higher than those of HCO_3^-, which may imply that (a) carbonate dissolution involves acids other than carbonic acid, and (b) evaporite dissolution provides extra sources of Ca and/or Mg. The addition of SO_4^{2-} can lead to a balance in the anions and cations, which indicates that additional sulfuric acid is dissolved with the carbonate to increase the DIC concentration in December (Figure 11b) (Jia et al., 2021). Precipitation research in the Yangtze River Basin showed little difference in SO_4^{2-} in rainfall in different seasons, which was much lower than in the river (Li et al., 2020a, 2020b; Yoon et al., 2008). Therefore, acid deposition caused by rainfall may not be a significant contributor to sulfuric acid in the middle and lower reaches. In contrast, the better correlation between metal cations (Na^+ and Mg^{2+}) and SO_4^{2-} in the water samples suggests that evaporation and dissolution of minerals such as mirabilite ($Na_2SO_4{\cdot}10H_2O$) and polyhalite ($MgSO_4$) were an additional sulfate source in December (Figures 11c and 11d) (Wang et al., 2022; Zhang et al., 2021). Abundant evaporite reserves in the two lake basins and the characteristics of evaporation, that is, easy crystallization in dry season, further support this hypothesis, as additional sulfuric acid increased the carbonate dissolution proportion of DIC in December (Chetelat et al., 2008). In addition, congruent calcite dissolution in the middle reach in December increased carbonate dissolution and produced more HCO_3^- than that in May (Figure 11e). Previous studies have shown that calcite has a faster dissolution rate than dolomite (Fairchild et al., 2000; Nash et al., 2013; Yadav et al., 2008), which further increased the seasonal difference in DIC in the middle reach (Equations 4 and 5).

Congruent dolomite dissolution:

$$CaMg(CO_3) + 2H_2CO_3 \rightarrow Ca^{2+} + Mg^{2+} + 4HCO_{3-} \quad (4)$$

Congruent calcite dissolution:

$$CaCO_3 + H_2CO_3 \rightarrow Ca^{2+} + 2HCO_{3-} \quad (5)$$

4.3. Effects of Environmental Factors on DIC and Its Sources

A significant correlation between environmental factors and DIC has been widely reported in global rivers (Kaijser et al., 2021; Liu et al., 2021). Redundancy analysis (RDA) showed that DIC in the upper reach of the Yangtze River mainly originated from carbonate dissolution and rock weathering with atmospheric CO_2 (Figure 12) (Chetelat et al., 2008; Zhang et al., 2014). Moreover, a positive correlation between the soil CO_2 proportion of DIC and organic carbon (OC, POC, and DOC) appeared in the RDA1 negative axis, where water samples were distributed in the lower reach (Figure 12; Table S7 in Supporting Information S1). This phenomenon indicates that the mineralization of organic matter increases the soil CO_2 proportion of DIC in the lower reach, and this effect is also evidenced by the significant positive correlation between OC and pCO_2 ($p < 0.01$) (Figure S13 in Supporting Information S1) (Dutta et al., 2019; Zhong et al., 2018). As the DOC concentration in the main stream of the Yangtze River has been increasing over the years, the variation in DIC concentration and source caused by OC transformation needs more attention. Moreover, higher water temperatures often enhance mineral weathering and promote DIC production (Liu et al., 2020; Prokushkin et al., 2011), but there was a significant negative correlation between water temperature and DIC in this study ($p < 0.01$) (Figure S13 in Supporting Information S1). This indicates that the variation in DIC is more sensitive to dam operation and lake recharge than to the warming effect on rock weathering. DIC accounts for 89.47% of total carbon, 93.48% of TDC, and 98.89% of inorganic carbon on average in this study. Mean DIC concentrations were higher after dam operation than before, which further highlights the disturbance of dam and river-lake exchange on watershed carbon cycle (Figure S14 in Supporting Information S1).

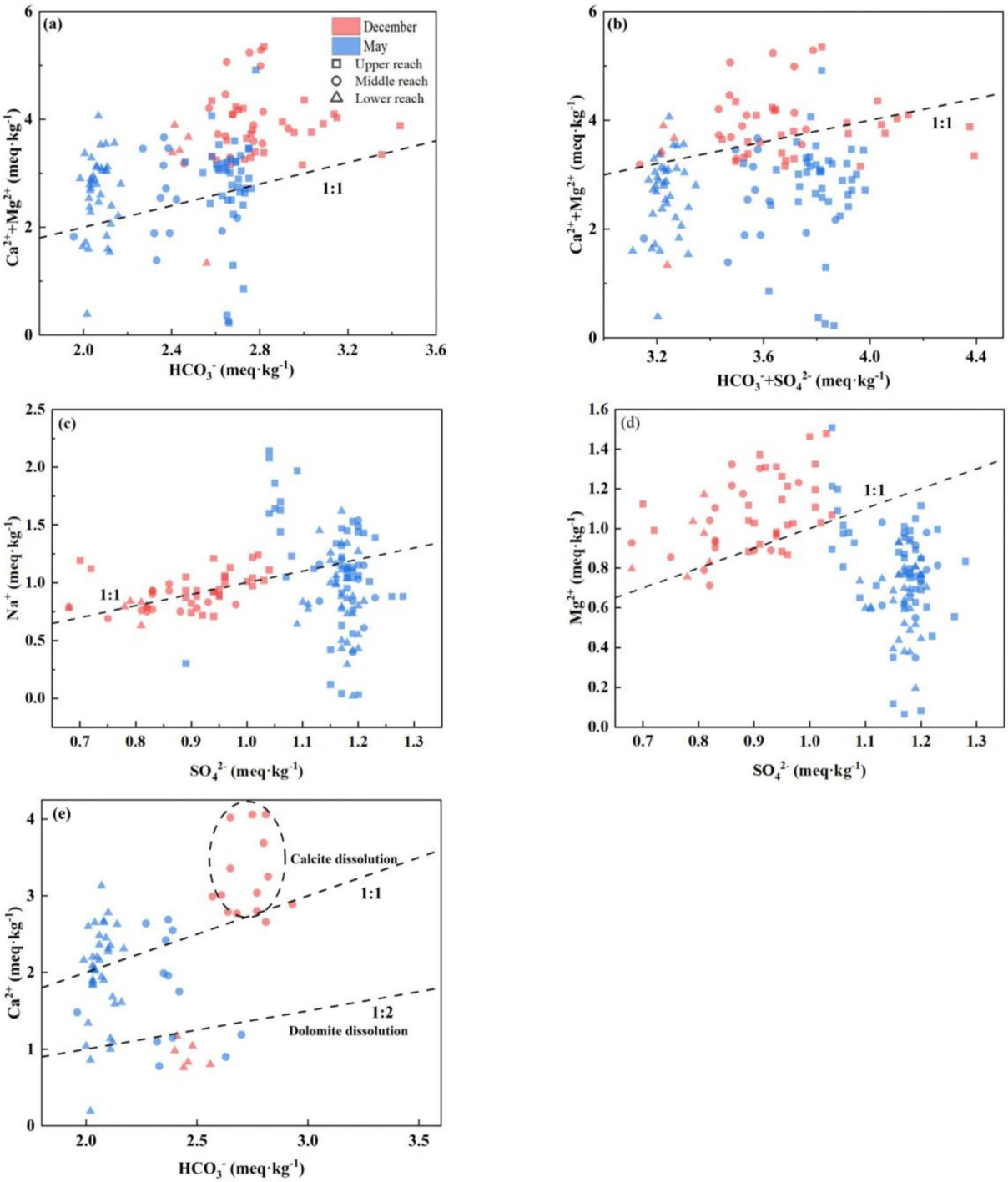

Figure 11. Stoichiometric relation among major ions in the main stream of the Yangtze River. (a) $Ca^{2+} + Mg^{2+}$ versus HCO_3^-; (b) $Ca^{2+} + Mg^{2+}$ versus $HCO_3^- + SO_4^{2-}$; (c) Na^+ versus SO_4^{2-}; (d) Mg^{2+} versus SO_4^{2-}; (e) Ca^{2+} versus HCO_3^-.

4.4. Impact of Dam on C-Q Relationship in Yangtze River and Other Rivers

High discharge often shortens the runoff transit time and depletes the DIC source supply (Liu et al., 2020; Wang et al., 2013; Zhong et al., 2021b). As with most Chinese rivers, previous studies have revealed that DIC concentrations (C) decreased with increasing discharge (Q) in the Yangtze River (C-Q relationships: $C = aQ^b$, where a and b are fitted parameters, b values near 0 indicate the chemostatic behavior of DIC with changing discharge)

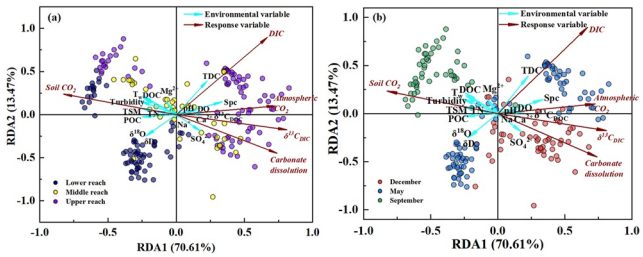

Figure 12. Redundancy analyses (RDA) for the $\delta^{13}C_{DIC,}$ DIC, and its source by environmental variables. (a) Score labels for distance and (b) score labels for month.

(Figure 13b) (Marinos et al., 2020; Zhong et al., 2020, 2021b). Notably, the *C-Q* relationship showed the chemostatic behavior after the TGD operation, with the value of *b* increasing and being close to 0 (Figures 13a and 13b). Before the TGD operation, increasing discharge had a dilution effect on the DIC in the main stream ($b < -0.20$) (Figure 13a), which represents a shortened fluid transit time, resulting in the depletion of the DIC supply (Zhong et al., 2021b). However, sediment mineralization increased the annual DIC in the TGR (Figure 9). On the other hand, the TGD operation gradually weakened the runoff supply downstream, and water was retained in the reservoir for sufficient time for water–rock reactions (Figure S15 in Supporting Information S1) (Deng et al., 2016). Increasing the DIC from the upper reach weakened the dilution effect of the lakes on the DIC in the middle and lower reaches, which contributed to the chemostatic relationship of *C-Q* in the main stream of the Yangtze River after the dam operation (Figure 13b). Therefore, dam operation has a profound effect on the fate of DIC exported from the main stream to the ocean.

Globally, dam operation may change the original chemical behavior of *Q* by impacting the transport and source limitations of DIC (Phuong et al., 2018; Tamooh et al., 2014). We investigated the long-term observation data of other rivers, and the fitting of *C-Q* in these rivers changed after dam operation (Figures 13c and 13d). The Jökulsá á Dal, Lagarfljót, and Fellsá rivers are located in eastern Iceland, which has a frigid-temperate marine

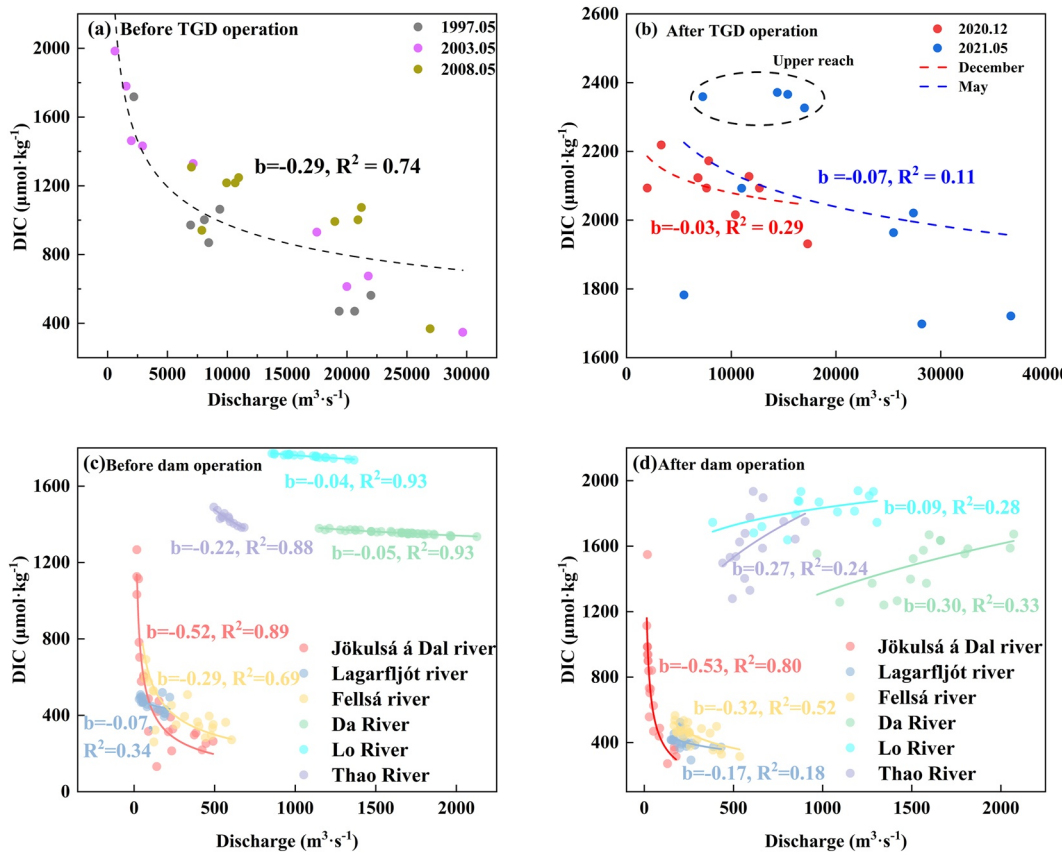

Figure 13. Correlation between DIC and discharge in the main stream of the Yangtze River, (a) data in this study; (b) data in the historical period; (c) data in global rivers before dam operation; and (d) data in global rivers after dam operation. Note that the data on DIC and discharge in May 1997, May 2003, and May 2008 from Zhang et al. (2014); the data on DIC in December 2020 and May 2021 from our study, and data on discharge from the hydrological station in the main stream of the Yangtze (http://113.57.190.228:8001); data of discharge and DIC in other global rivers from Eiriksdottir et al. (2017) and Phuong et al. (2018).

climate and basalt bedrock (Eiriksdottir et al., 2017). When dams release water and increase the discharge scour of the basalt bedrock, the shortened fluid transit time contributes to the depletion of DIC; thus, the DIC concentration is diluted by an increase in discharge after dam operation (the *b* value becomes negative) (Figure 13d). Da River, Lo River, and Thao River are located in the Red River basin of Vietnam, which has a tropical monsoon climate and carbonatite bedrock (Phuong et al., 2018). Carbonate weathering is the main source of HCO_3^-, and the higher discharge intensifies chemical weathering by increasing the reactive surface area. Therefore, the DIC showed the enrichment behavior with increasing discharge after dam operation, which differed from that of other rivers ($b > 0$) (Figure 13d). These results highlight that the geology of the watershed and damming change the chemostatic behavior of *C*-*Q*. With the increasing number of dams built worldwide and the frequent occurrence of extreme weather caused by global warming, the transport conditions of solutes will change greatly (Castello & Macedo, 2016; Haddeland et al., 2014), in watersheds with widespread minerals with fast carbonate weathering kinetics, the DIC will increase with increasing discharge. This study provides a framework for better understanding the transmission and transformation processes of DIC in river–reservoir systems.

5. Conclusion

In this study, isotope tracing and hydrochemical analysis methods were used to interpret the influence of dam operation and lake recharge on DIC. DIC in the reservoir area reached 2,269.94 μmol kg^{-1} and then decreased by 7.77% and 21.95% after the inflow of Dongting Lake and Poyang Lake, respectively, into the main stream. $\delta^{13}C_{DIC}$ analyzed using Bayesian mixture model indicated that DIC originates from rock weathering (involved carbonate dissolution and atmospheric CO_2) and soil CO_2 generated by organic matter mineralization. Lake recharge weakened the rock weathering process such that the carbonate dissolution and atmospheric CO_2 proportions of DIC decreased from the upper reach to the lower reach. Meanwhile, terrestrial substance transported from lakes increased the soil CO_2 proportion of DIC in middle and lower reach of the Yangtze River. The regulation of TGD on DIC was found to be seasonally independent in upper reach of the Yangtze River. During the dry season, the DIC decreases in the TGD area, dominated by CO_2 degassing and calcite precipitation. In the wet season, a lower CV of d-excess revealed a longer runoff retention time in the reservoir, leading to sufficient water–rock interactions to increase the DIC and the proportion of DIC from carbonate dissolution. Enrichment of $\delta^{18}O$ from the middle to lower reaches revealed the flow of lakes mixed into the main stream of the Yangtze River, which decreased the DIC concentration and the source proportion of carbonate dissolution. Globally, the impact of damming on the DIC transmission process was evaluated among the Yangtze River and other rivers, and damming in watersheds with different geologies has limited the transport and source of DIC, thereby further altering the original chemostatic behavior of *C*-*Q*. Future studies should focus on the effects of damming and lake recharge on chemical weathering in watersheds. Research on chemical weathering processes under a variety of geologies is also needed to better understand the transmission and transformation processes of DIC in the river–ocean continuum.

Conflict of Interest

The authors declare no conflicts of interest relevant to this study.

Data Availability Statement

Data Citation: The original data related to this article about water chemical parameters in the Yangtze River are available on the website of Zenodo (Zhao, 2023, https://doi.org/10.5281/zenodo.8273583). *Software Citation*: Stock (2020), https://rdocumentation.org/packages/MixSIAR/versions/3.1.12.

Acknowledgments
This study was supported by the National Natural Science Foundation of China (Grants 42277214, 41971286, and 41773097), major programs of the National Social Science Foundation of China (Grant 22&ZD136), Special Science and Technology Innovation Program for Carbon Peak and Carbon Neutralization of Jiangsu Province (Grant BE2022612) and the Postgraduate Research Innovation Project of Jiangsu Province (KYCX22_1562).

References

Abongwa, P. T., & Atekwana, E. A. (2015). Controls on the chemical and isotopic composition of carbonate springs during evolution to saturation with respect to calcite. *Chemical Geology*, *404*, 136–149. https://doi.org/10.1016/j.chemgeo.2015.03.024

Abongwa, P. T., & Atekwana, E. A. (2018). A laboratory study investigating the effects of dilution by precipitation on dissolved inorganic carbon and stable isotope evolution in surface waters. *Environmental Science & Pollution Research*, *25*(20), 19941–19952. https://doi.org/10.1007/s11356-018-2085-0

Akhand, A., Watanabe, K., Chanda, A., Tokoro, T., Chakraborty, K., Moki, H., et al. (2021). Lateral carbon fluxes and CO_2 evasion from a subtropical mangrove-seagrass-coral continuum. *Science of the Total Environment*, *752*, 142190. https://doi.org/10.1016/j.scitotenv.2020.142190

Amini, A., & Alimohammadlou, M. (2021). Toward equation structural modeling: An integration of interpretive structural modeling and structural equation modeling. *Journal of Management Analytics*, *8*(4), 693–714. https://doi.org/10.1080/23270012.2021.1881927

Amiotte-Suchet, P., Aubert, D., Probst, J. L., Gauthier-Lafaye, F., Probst, A., Andreux, F., & Viville, D. (1999). $\delta^{13}C$ pattern of dissolved inorganic carbon in a small granitic catchment: The Strengbach case study (Vosges mountains, France). *Chemical Geology*, *159*(1–4), 129–145. https://doi.org/10.1016/s0009-2541(99)00037-6

Aufdenkampe, A. K., Mayorga, E., Raymond, P. A., Melack, J. M., Doney, S. C., Alin, S. R., et al. (2011). Riverine coupling of biogeochemical cycles between land, oceans, and atmosphere. *Frontiers in Ecology and the Environment*, *9*(1), 53–60. https://doi.org/10.1890/100014

Cai, Y., Guo, L., Wang, X., & Aiken, G. (2015). Abundance, stable isotopic composition, and export fluxes of DOC, POC, and DIC from the Lower Mississippi River during 2006-2008. *Journal of Geophysical Research: Biogeosciences*, *120*(11), 2273–2288. https://doi.org/10.1002/2015jg003139

Campeau, A., & Del Giorgio, P. A. (2014). Patterns in CH_4 and CO_2 concentrations across boreal rivers: Major drivers and implications for fluvial greenhouse emissions under climate change scenarios. *Global Change Biology*, *20*(4), 1075–1088. https://doi.org/10.1111/gcb.12479

Cao, X., Wu, P., Han, Z., Tu, H., & Zhang, S. (2016). Factors controlling the isotope composition of dissolved inorganic carbon in a karst-dominated wetland catchment, Guizhou Province, Southwest China. *Journal of Marine Systems*, *75*, 1–14. https://doi.org/10.1007/s12665-016-5899-4

Castello, L., & Macedo, M. N. (2016). Large-scale degradation of Amazonian freshwater ecosystems. *Global Change Biology*, *22*(3), 990–1007. https://doi.org/10.1111/gcb.13173

Catalán, N., Marcé, R., Kothawala, D. N., & Tranvik, L. J. (2016). Organic carbon decomposition rates controlled by water retention time across inland waters. *Nature Geoscience*, *9*(7), 501–504. https://doi.org/10.1038/ngeo2720

Chen, S., Zhong, J., Li, C., Liu, J., Wang, W., Xu, S., & Li, S. L. (2021). Coupled effects of hydrology and temperature on temporal dynamics of dissolved carbon in the Min River, Tibetan Plateau. *Journal of Hydrology*, *593*, 125641. https://doi.org/10.1016/j.jhydrol.2020.125641

Chetelat, B., Liu, C. Q., Zhao, Z. Q., Wang, Q. L., Li, S. L., Li, J., & Wang, B. L. (2008). Geochemistry of the dissolved load of the Changjiang Basin rivers: Anthropogenic impacts and chemical weathering. *Geochimica et Cosmochimica Acta*, *72*(17), 4254–4277. https://doi.org/10.1016/j.gca.2008.06.013

Cole, J. J., Prairie, Y. T., Caraco, N. F., McDowell, W. H., Tranvik, L. J., Striegl, R. G., et al. (2007). Plumbing the global carbon cycle: Integrating inland waters into the terrestrial carbon budget. *Ecosystems*, *10*(1), 171–184. https://doi.org/10.1007/s10021-006-9013-8

Cotovicz, L. C., Knoppers, B. A., Deirmendjian, L., & Abril, G. (2019). Sources and sinks of dissolved inorganic carbon in an urban tropical coastal bay revealed by $\delta^{13}C$-DIC signals. *Estuarine, Coastal and Shelf Science*, *220*, 185–195. https://doi.org/10.1016/j.ecss.2019.02.048

Craig, H. (1961). Isotopic variations in meteoric waters. *Science*, *133*(3465), 1702–1703. https://doi.org/10.1126/science.133.3465.1702

Deng, K., Yang, S., Lian, E., Li, C., Yang, C., & Wei, H. (2016). Three Gorges Dam alters the Changjiang (Yangtze) river water cycle in the dry seasons: Evidence from H-O isotopes. *Science of the Total Environment*, *562*, 89–97. https://doi.org/10.1016/j.scitotenv.2016.03.213

Ding, T., Gao, J., Tian, S., Shi, G., Chen, F., Wang, C., et al. (2014). Chemical and isotopic characteristics of the water and suspended particulate materials in the Yangtze River and their geological and environmental implications. *Acta Geologica Sinica*, *88*(1), 276–360. https://doi.org/10.1111/1755-6724.12197

Drake, T. W., Raymond, P. A., & Spencer, R. G. M. (2018). Terrestrial carbon inputs to inland waters: A current synthesis of estimates and uncertainty. *Limnology & Oceanography*, *3*, 132–142. https://doi.org/10.1002/lol2.10055

Dutta, M. K., Kumar, S., Mukherjee, R., Sharma, N., Acharya, A., Sanyal, P., et al. (2019). Diurnal carbon dynamics in a mangrove-dominated tropical estuary (Sundarbans, India). *Estuarine, Coastal and Shelf Science*, *229*, 106426. https://doi.org/10.1016/j.ecss.2019.106426

Duvert, C., Hutley, L. B., Birkel, C., Rudge, M., Munksgaard, N. C., Wynn, J. G., et al. (2020). Seasonal shift from biogenic to geogenic fluvial carbon caused by changing water sources in the wet-dry tropics. *Journal of Geophysical Research: Biogeosciences*, *125*(2), 1–14. https://doi.org/10.1029/2019jg005384

Eiriksdottir, E. S., Oelkers, E. H., Hardardottir, J., & Gislason, S. R. (2017). The impact of damming on riverine fluxes to the ocean: A case study from eastern Iceland. *Water Research*, *113*, 124–138. https://doi.org/10.1016/j.watres.2016.12.029

Evans, M., Hastings, N., & Peacock, B. (2000). *Statistical distributions*. John Wiley & Sons.

Fairchild, I. J., Borsato, A., Tooth, A. F., Frisia, S., Hawkesworth, C. J., Huang, Y., et al. (2000). Controls on trace element (Sr-Mg) compositions of carbonate cave waters: Implications for speleothem climatic records. *Chemical Geology*, *166*(3–4), 255–269. https://doi.org/10.1016/s0009-2541(99)00216-8

Gao, Y., Jia, J., Lu, Y., Yang, T., Lyu, S., Shi, K., et al. (2021). Determining dominating control mechanisms of inland water carbon cycling processes and associated gross primary productivity on regional and global scales. *Earth-Science Reviews*, *213*, 103497. https://doi.org/10.1016/j.earscirev.2020.103497

Gao, Y., Jia, J., Lu, Y., Zhou, F., Hao, Z., Johnes, P. J., et al. (2020). Cascading multiscale watershed effects on differential carbon isotopic characteristics and associated hydrological processes. *Journal of Hydrology*, *588*, 125139. https://doi.org/10.1016/j.jhydrol.2020.125139

Gao, Y., Wang, S., Lu, Y., Liu, J., Lyu, S., Sun, K., et al. (2022). Carbon budget and balance critical processes of the regional land-water-air interface: Indicating the Earth system's carbon neutrality. *Science China Earth Sciences*, *65*(5), 773–782. https://doi.org/10.1007/s11430-021-9883-3

Gordeev, V. V., Martin, J. M., Sidorov, I. S., & Sidorova, M. V. (1996). A reassessment of the Eurasian river input of water, sediment, major elements, and nutrients to the Arctic Ocean. *American Journal of Science*, *296*(6), 664–691. https://doi.org/10.2475/ajs.296.6.664

Gu, Y., Tobino, T., & Nakajima, F. (2020). Effect of calcite saturation state on the growth and mortality of Heterocypris incongruens and a proposal for an reference artificial sediment in the sediment toxicity test ISO14371. *Science of the Total Environment*, *702*, 134993. https://doi.org/10.1016/j.scitotenv.2019.134993

Guo, J., Xie, Y., Guan, A., Qi, W., Cao, X., Peng, J., et al. (2023). Dam construction reshapes sedimentary pollutant distribution along the Yangtze River by regulating sediment composition. *Environment and Pollution*, *316*, 120659. https://doi.org/10.1016/j.envpol.2022.120659

Guo, S., Xiong, L., Zha, X., Zeng, L., & Cheng, L. (2021). Impacts of the Three Gorges Dam on the streamflow fluctuations in the downstream region. *Journal of Hydrology*, *598*, 126480. https://doi.org/10.1016/j.jhydrol.2021.126480

Haddeland, I., Heinke, J., Biemans, H., Eisner, S., Flörke, M., Hanasaki, N., et al. (2014). Global water resources affected by human interventions and climate change. *Proceedings of the National Academy of Sciences of the United States of America*, *111*(9), 3251–3256. https://doi.org/10.1073/pnas.1222475110

Han, Q., Wang, B., Liu, C. Q., Wang, F., Peng, X., & Liu, X. L. (2018). Carbon biogeochemical cycle is enhanced by damming in a karst river. *Science of the Total Environment*, *616–617*, 1181–1189. https://doi.org/10.1016/j.scitotenv.2017.10.202

Herath, I. K., Wu, S., Ma, M., & Huang, P. (2020). Reservoir CO_2 evasion flux and controlling factors of carbon species traced by $\delta^{13}C$DIC at different regulating phases of a hydro-power dam. *Science of the Total Environment*, *698*, 134184. https://doi.org/10.1016/j.scitotenv.2019.134184

Herath, I. K., Wu, S., Ma, M., & Ping, H. (2022). Dynamic of riverine pCO_2, biogeochemical characteristics, and carbon sources inferred from $\delta^{13}C$ in a subtropical river system. *Science of the Total Environment*, *821*, 153296. https://doi.org/10.1016/j.scitotenv.2022.153296

Huang, C., Meng, L., He, Y., Shang, N., Yu, H., Huang, T., et al. (2022). Spatial variation of particulate black carbon, and its sources in a large eutrophic urban lake in China. *Science of the Total Environment*, *803*, 150057. https://doi.org/10.1016/j.scitotenv.2021.150057

Huang, C., Yao, L., Zhang, Y., Huang, T., Zhang, M., Zhu, A. X., & Yang, H. (2017). Spatial and temporal variation in autochthonous and allochthonous contributors to increased organic carbon and nitrogen burial in a plateau lake. *Science of the Total Environment*, *603–604*, 390–400. https://doi.org/10.1016/j.scitotenv.2017.06.118

Huang, C., Zhang, L., Li, Y., Lin, C., Huang, T., Zhang, M., et al. (2018). Carbon and nitrogen burial in a plateau lake during eutrophication and phytoplankton blooms. *Science of the Total Environment*, *616–617*, 296–304. https://doi.org/10.1016/j.scitotenv.2017.10.320

Isaji, Y., Kawahata, H., Kuroda, J., Yoshimura, T., Ogawa, N. O., Suzuki, A., et al. (2017). Biological and physical modification of carbonate system parameters along the salinity gradient in shallow hypersaline solar salterns in Trapani, Italy. *Geochimica et Cosmochimica Acta*, *208*, 354–367. https://doi.org/10.1016/j.gca.2017.04.013

Ishikawa, N. F., Tayasu, I., Yamane, M., Yokoyama, Y., Sakai, S., & Ohkouchi, N. (2015). Sources of dissolved inorganic carbon in two small streams with different bedrock geology: Insights from carbon isotopes. *Radiocarbon*, *57*(3), 439–448. https://doi.org/10.2458/azu_rc.57.18348

Jia, H., Qu, W., Ren, W., & Qian, H. (2021). Impacts of chemical weathering and human perturbations on dissolved loads of the Wei River, the Yellow River catchment. *Journal of Hydrology*, *603*, 126950. https://doi.org/10.1016/j.jhydrol.2021.126950

Kaijser, W., Lorenz, A. W., Birk, S., & Hering, D. (2021). The interplay of nutrients, dissolved inorganic carbon and algae in determining macrophyte occurrences in rivers. *Science of the Total Environment*, *781*, 146728. https://doi.org/10.1016/j.scitotenv.2021.146728

Kapetanaki, N., Krasakopoulou, E., Stathopoulou, E., Dassenakis, M., & Scoullos, M. (2020). Severe coastal hypoxia interchange with ocean acidification: An experimental perturbation study on carbon and nutrient biogeochemistry. *Journal of Marine Science and Engineering*, *8*(6), 1–20. https://doi.org/10.3390/jmse8060462

Kapetanaki, N., Krasakopoulou, E., Stathopoulou, E., Pavlidou, A., Zervoudaki, S., Dassenakis, M., & Scoullos, M. (2018). Simulation of coastal processes affecting pH with impacts on carbon and nutrient biogeochemistry. *Mediterranean Marine Science*, *19*, 290–304. https://doi.org/10.12681/mms.14439

Leybourne, M. I., Clark, I. D., & Goodfellow, W. D. (2006). Stable isotope geochemistry of ground and surface waters associated with undisturbed massive sulfide deposits; constraints on origin of waters and water-rock reactions. *Chemical Geology*, *231*(4), 300–325. https://doi.org/10.1016/j.chemgeo.2006.02.004

Li, J., Pu, J., & Zhang, T. (2022). Transport and transformation of dissolved inorganic carbon in a subtropical groundwater-fed reservoir, South China. *Water Research*, *209*, 117905. https://doi.org/10.1016/j.watres.2021.117905

Li, J., Song, F., Bao, Z., Fan, H., & Wu, H. (2022). Insights into shallow freshwater lakes hydrology in the Yangtze floodplain from stable water isotope tracers. *Water (Switzerland)*, *14*(3), 1–14. https://doi.org/10.3390/w14030506

Li, Z., Li, Z., Feng, Q., Zhang, B., Gui, J., Xue, J., & Gao, W. (2020a). Runoff dominated by supra-permafrost water in the source region of the Yangtze River using environmental isotopes. *Journal of Hydrology*, *582*, 124506. https://doi.org/10.1016/j.jhydrol.2019.124506

Li, S., Ni, M., Mao, R., & Bush, R. T. (2018). Riverine CO_2 supersaturation and outgassing in a subtropical monsoonal mountainous area (Three Gorges Reservoir Region) of China. *Journal of Hydrology*, *558*, 460–469. https://doi.org/10.1016/j.jhydrol.2018.01.057

Li, S., Xu, Y. J., & Ni, M. (2021). Changes in sediment, nutrients and major ions in the world largest reservoir: Effects of damming and reservoir operation. *Journal of Cleaner Production*, *318*, 128601. https://doi.org/10.1016/j.jclepro.2021.128601

Li, Z., Sun, Z., Chen, Y., Li, C., Pan, Z., Harby, A., et al. (2020b). The net GHG emissions of the China Three Gorges Reservoir: I. Pre-impoundment GHG inventories and carbon balance. *Journal of Cleaner Production*, *256*, 120635. https://doi.org/10.1016/j.jclepro.2020.120635

Liu, J., Zhong, J., Chen, S., Xu, S., & Li, S. L. (2021). Hydrological and biogeochemical controls on temporal variations of dissolved carbon and solutes in a karst river, South China. *Environmental Sciences Europe*, *33*(1), 53. https://doi.org/10.1186/s12302-021-00495-x

Liu, J., Zhong, J., Ding, H., Yue, F. J., Li, C., Xu, S., & Li, S. L. (2020). Hydrological regulation of chemical weathering and dissolved inorganic carbon biogeochemical processes in a monsoonal river. *Hydrological Processes*, *34*(12), 2780–2792. https://doi.org/10.1002/hyp.13763

Liu, S. D., Lu, X. X., Xia, X. H., Zhang, S. R., Ran, L. S., Yang, X. K., & Liu, T. (2016). Dynamic biogeochemical controls on river pCO_2 and recent changes under aggravating river impoundment: An example of the subtropical Yangtze River. *Global Biogeochemical Cycles*, *30*(6), 880–897. https://doi.org/10.1002/2016gb005388

Lu, W., Wang, S., Yeager, K. M., Liu, F., Huang, Q., Yang, Y., et al. (2018). Importance of considered organic versus inorganic source of carbon to lakes for calculating net effect on landscape C budgets. *Journal of Geophysical Research: Biogeosciences*, *123*(4), 1302–1317. https://doi.org/10.1002/2017jg004159

Lu, Y., Gao, Y., Dungait, J. A. J., Jia, J., Sun, K., Wang, S., et al. (2022). Understanding how inland lake system environmental gradients on the Qinghai-Tibet Plateau impact the geographical patterns of carbon and water sources or sink. *Journal of Hydrology*, *604*, 127219. https://doi.org/10.1016/j.jhydrol.2021.127219

Maavara, T., Lauerwald, R., Regnier, P., & Cappellen, P. V. (2017). Global perturbation of organic carbon cycling by river damming. *Nature Communications*, *8*(1), 15347. https://doi.org/10.1038/ncomms15347

Marinos, R. E., Van Meter, K. J., & Basu, N. B. (2020). Is the river a chemostat? Scale versus land use controls on nitrate concentration-discharge dynamics in the Upper Mississippi River Basin. *Geophysical Research Letters*, *47*(16), 1–11. https://doi.org/10.1029/2020GL087051

Marx, A., Dusek, J., Jankovec, J., Sanda, M., Vogel, T., van Geldern, R., et al. (2017). A review of CO_2 and associated carbon dynamics in headwater streams: A global perspective. *Reviews of Geophysics*, *55*(2), 560–585. https://doi.org/10.1002/2016rg000547

Mendonça, R., Müller, R. A., Clow, D., Verpoorter, C., Raymond, P., Tranvik, L. J., & Sobek, S. (2017). Organic carbon burial in global lakes and reservoirs. *Nature Communications*, *8*, 1–6. https://doi.org/10.1038/s41467-017-01789-6

Nakayama, K., Kawahara, Y., Kurimoto, Y., Tada, K., Lin, H. C., Hung, M. C., et al. (2022). Effects of oyster aquaculture on carbon capture and removal in a tropical mangrove lagoon in southwestern Taiwan. *Science of the Total Environment*, *838*, 156460. https://doi.org/10.1016/j.scitotenv.2022.156460

Nash, M. C., Opdyke, B. N., Troitzsch, U., Russell, B. D., Adey, W. H., Kato, A., et al. (2013). Dolomite-rich coralline algae in reefs resist dissolution in acidified conditions. *Nature Climate Change*, *3*, 268–272. https://doi.org/10.1038/nclimate1760

Papadimitriou, S., Kennedy, H., Kennedy, D. P., & Borum, J. (2005). Seasonal and spatial variation in the organic carbon and nitrogen concentration and their stable isotopic composition in *Zostera* marina (Denmark). *Limnology & Oceanography*, *50*(4), 1084–1095. https://doi.org/10.4319/lo.2005.50.4.1084

Phuong, T., Le, Q., Da, N., Viet, L., Dao, N., Rochelle, E., et al. (2018). Change in carbon flux (1960–2015) of the Red River (Vietnam). *Environmental Earth Sciences*, *77*, 1–18. https://doi.org/10.1007/s12665-018-7851-2

Pierrot, D., Lewis, E., & Wallace, D. (2006). *ORNL/CDIAC-105a. Carbon dioxide information analysis center*. Oak Ridge National Laboratory, US Department of Energy.

Pipko, I. I., Pugach, S. P., Savichev, O. G., Repina, I. A., Shakhova, N. E., Moiseeva, Y. A., et al. (2019). Dynamics of dissolved inorganic carbon and CO_2 fluxes between the water and the atmosphere in the main channel of the Ob River. *Doklady Akademii Nauk*, *484*(2), 52–57. https://doi.org/10.1134/s0012500819020101

Probst, J. L., Mortatti, J., & Tardy, Y. (1994). Carbon river fluxes and weathering CO_2 consumption in the Congo and Amazon river basins. *Applied Geochemistry*, *9*, 1–13. https://doi.org/10.1016/0883-2927(94)90047-7

Prokushkin, A. S., Pokrovsky, O. S., Shirokova, L. S., Korets, M. A., Viers, J., Prokushkin, S. G., et al. (2011). Sources and the flux pattern of dissolved carbon in rivers of the Yenisey basin draining the Central Siberian Plateau. *Environmental Research Letters*, *6*(4), 045212. https://doi.org/10.1088/1748-9326/6/4/045212

Pu, J., Li, J., Khadka, M. B., Martin, J. B., Zhang, T., Yu, S., & Yuan, D. (2017). In-stream metabolism and atmospheric carbon sequestration in a groundwater-fed karst stream. *Science of the Total Environment*, *579*, 1343–1355. https://doi.org/10.1016/j.scitotenv.2016.11.132

Raymond, P. A., & Hamilton, S. K. (2018). Anthropogenic influences on riverine fluxes of dissolved inorganic carbon to the oceans. *Limnology and Oceanography Letters*, *3*, 143–155. https://doi.org/10.1002/lol2.10069

Raymond, P. A., Hartmann, J., Lauerwald, R., Sobek, S., McDonald, C., Hoover, M., et al. (2013). Global carbon dioxide emissions from inland waters. *Nature*, *503*(7476), 355–359. https://doi.org/10.1038/nature12760

Reyes-Macaya, D., Hoogakker, B., Martínez-Méndez, G., Llanillo, P. J., Grasse, P., Mohtadi, M., et al. (2022). Isotopic characterization of water masses in the southeast Pacific region: Paleoceanographic implications. *Journal of Geophysical Research: Oceans*, *127*(1), e2021JC017525. https://doi.org/10.1029/2021jc017525

Rice, E. W., Baird, R. B., Eaton, A. D., & Clesceri, L. S. (2012). *Standard methods for the examination of water and wastewater*. American Public Health Association.

Samanta, S., Dalai, T. K., Pattanaik, J. K., Rai, S. K., & Mazumdar, A. (2015). Dissolved inorganic carbon (DIC) and its $\delta^{13}C$ in the Ganga (Hooghly) River estuary, India: Evidence of DIC generation via organic carbon degradation and carbonate dissolution. *Geochimica et Cosmochimica Acta*, *165*, 226–248. https://doi.org/10.1016/j.gca.2015.05.040

Shan, S., Luo, C., Qi, Y., Cai, W. J., Sun, S., Fan, D., & Wang, X. (2021). Carbon isotopic and lithologic constraints on the sources and cycling of inorganic carbon in four large rivers in China: Yangtze, Yellow, Pearl, and Heilongjiang. *Journal of Geophysical Research: Biogeosciences*, *126*(2), e2020JG005901. https://doi.org/10.1029/2020jg005901

Song, C., Wang, G., Mao, T., Huang, K., Sun, X., Hu, Z., et al. (2020). Spatiotemporal variability and sources of DIC in permafrost catchments of the Yangtze River source region: Insights from stable carbon isotope and water chemistry. *Water Resources Research*, *56*(1), e2019WR025343. https://doi.org/10.1029/2019wr025343

Song, X. W., Lyu, S. D., Sun, K., Gao, Y., & Wen, X. F. (2021). Flux and source of dissolved inorganic carbon in a headwater stream in a subtropical plantation catchment. *Journal of Hydrology*, *600*, 126511. https://doi.org/10.1016/j.jhydrol.2021.126511

Stock, B. (2020). Analysis of DIC isotope source were made with MixSIAR model: October 20, 2020 release (versions 3.1.12.) [Software]. Rdocumentation. https://rdocumentation.org/packages/MixSIAR/versions/3.1.12

Su, J., Cai, W. J., Hussain, N., Brodeur, J., Chen, B., & Huang, K. (2019). Simultaneous determination of dissolved inorganic carbon (DIC) concentration and stable isotope ($\delta^{13}C$-DIC) by Cavity Ring-Down Spectroscopy: Application to study carbonate dynamics in the Chesapeake Bay. *Marine Chemistry*, *215*, 103689. https://doi.org/10.1016/j.marchem.2019.103689

Tamooh, F., Meysman, F. J. R., Borges, A. V., Marwick, T. R., Van Den Meersche, K., Dehairs, F., et al. (2014). Sediment and carbon fluxes along a longitudinal gradient in the lower Tana River (Kenya). *Journal of Geophysical Research: Biogeosciences*, *119*(7), 1340–1353. https://doi.org/10.1002/2013jg002358

Telmer, K., & Veizer, J. (1999). Carbon fluxes, pCO_2 and substrate weathering in a large northern river basin, Canada: Carbon isotope perspectives. *Chemical Geology*, *159*(1–4), 61–86. https://doi.org/10.1016/s0009-2541(99)00034-0

Uthicke, S., & Fabricius, K. E. (2012). Productivity gains do not compensate for reduced calcification under near-future ocean acidification in the photosynthetic benthic foraminifer species Marginopora vertebralis. *Global Change Biology*, *18*(9), 2781–2791. https://doi.org/10.1111/j.1365-2486.2012.02715.x

van Hoek, W. J., Wang, J., Vilmin, L., Beusen, A. H. W., Mogollón, J. M., Müller, G., et al. (2021). Exploring spatially explicit changes in carbon budgets of global river basins during the 20th century. *Environmental Science & Technology*, *55*(24), 16757–16769. https://doi.org/10.1021/acs.est.1c04605

Voss, B. M., Wickland, K. P., Aiken, G. R., & Striegl, R. G. (2017). Biological and land use controls on the isotopic composition of aquatic carbon in the Upper Mississippi River Basin. *Global Biogeochemical Cycles*, *31*(8), 1271–1288. https://doi.org/10.1002/2017gb005699

Wang, G., Jiang, T., Blender, R., & Fraedrich, K. (2008). Yangtze 1/f discharge variability and the interacting river-lake system. *Journal of Hydrology*, *351*(1–2), 230–237. https://doi.org/10.1016/j.jhydrol.2007.12.016

Wang, M., Yang, L., Li, J., & Liang, Q. (2022). Hydrochemical characteristics and controlling factors of surface water in Upper Nujiang River, Qinghai-Tibet Plateau. *Minerals*, *12*(4), 490. https://doi.org/10.3390/min12040490

Wang, W., Li, S. L., Zhong, J., Li, C., Yi, Y., Chen, S., & Ren, Y. (2019). Understanding transport and transformation of dissolved inorganic carbon (DIC)in the reservoir system using $\delta^{13}C_{DIC}$ and water chemistry. *Journal of Hydrology*, *574*, 193–201. https://doi.org/10.1016/j.jhydrol.2019.04.036

Wang, W. F., Li, S. L., Zhong, J., Maberly, S. C., Li, C., Wang, F. S., et al. (2020). Climatic and anthropogenic regulation of carbon transport and transformation in a karst river-reservoir system. *Science of the Total Environment*, *707*, 135628. https://doi.org/10.1016/j.scitotenv.2019.135628

Wang, X., Luo, C., Ge, T., Xu, C., & Xue, Y. (2016). Controls on the sources and cycling of dissolved inorganic carbon in the Changjiang and Huanghe River estuaries, China: ^{14}C and ^{13}C studies. *Limnology & Oceanography*, *61*(4), 1358–1374. https://doi.org/10.1002/lno.10301

Wang, Z. A., Bienvenu, D. J., Mann, P. J., Hoering, K. A., Poulsen, J. R., Spencer, R. G. M., & Holmes, R. M. (2013). Inorganic carbon speciation and fluxes in the Congo River. *Geophysical Research Letters*, *40*(3), 511–516. https://doi.org/10.1002/grl.50160

Wen, Z., Shang, Y., Lyu, L., Li, S., Tao, H., & Song, K. (2021). A review of quantifying pCO_2 in inland waters with a global perspective: Challenges and prospects of implementing remote sensing technology. *Remote Sensing*, *13*(23), 4916. https://doi.org/10.3390/rs13234916

Wu, H., Song, F., Li, J., Zhou, Y., Zhang, J., & Fu, C. (2022). Surface water isoscapes ($\delta^{18}O$ and $\delta^{2}H$) reveal dual effects of damming and drought on the Yangtze River water cycles. *Journal of Hydrology*, *610*, 127847. https://doi.org/10.1016/j.jhydrol.2022.127847

Wu, Q., & Han, G. (2018). $\delta^{13}C_{DIC}$ tracing of dissolved inorganic carbon sources at Three Gorges Reservoir, China. *Water Science and Technology*, *77*(2), 555–564. https://doi.org/10.2166/wst.2017.577

Wu, S., & Firoozabadi, A. (2010). Permanent alteration of porous media wettability from liquid-wetting to intermediate gas-wetting. *Transport in Porous Media*, *85*(1), 189–213. https://doi.org/10.1007/s11242-010-9554-3

Xu, Y. J., Xu, Z., & Yang, R. (2019). Rapid daily change in surface water pCO_2 and CO_2 evasion: A case study in a subtropical eutrophic lake in southern USA. *Journal of Hydrology*, *570*, 486–494. https://doi.org/10.1016/j.jhydrol.2019.01.016

Yadav, S. K., Chakrapani, G. J., & Gupta, M. K. (2008). An experimental study of dissolution kinetics of Calcite, Dolomite, Leucogranite and Gneiss in buffered solutions at temperature 25 and 5°C. *Environmental Geology*, *53*(8), 1683–1694. https://doi.org/10.1007/s00254-007-0775-x

Yang, S. L., Milliman, J. D., Xu, K. H., Deng, B., Zhang, X. Y., & Luo, X. X. (2014). Downstream sedimentary and geomorphic impacts of the Three Gorges Dam on the Yangtze River. *Earth-Science Reviews*, *138*, 469–486. https://doi.org/10.1016/j.earscirev.2014.07.006

Yoon, J., Huh, Y., Lee, I., Moon, S., Noh, H., & Qin, J. (2008). Weathering processes in the Min Jiang: Major elements, $^{87}Sr/^{86}Sr$, $\delta^{34}S_{SO4}$, and $\delta^{18}O_{SO4}$. *Aquatic Geochemistry*, *14*(2), 147–170. https://doi.org/10.1007/s10498-008-9030-7

Zachara, J. M., Moran, J. J., Resch, C. T., Lindemann, S. R., Felmy, A. R., Bowden, M. E., et al. (2016). Geo- and biogeochemical processes in a heliothermal hypersaline lake. *Geochimica et Cosmochimica Acta*, *181*, 144–163. https://doi.org/10.1016/j.gca.2016.02.001

Zeng, S., Liu, H., Liu, Z., Kaufmann, G., Zeng, Q., & Chen, B. (2019). Seasonal and diurnal variations in DIC, NO_3^- and TOC concentrations in spring-pond ecosystems under different land-uses at the Shawan Karst Test Site, SW China: Carbon limitation of aquatic photosynthesis. *Journal of Hydrology*, *574*, 811–821. https://doi.org/10.1016/j.jhydrol.2019.04.090

Zhang, L., Xue, M., Wang, M., Cai, W. J., Wang, L., & Yu, Z. (2014). The spatiotemporal distribution of dissolved inorganic and organic carbon in the main stem of the Changjiang (Yangtze) River and the effect of the Three Gorges Reservoir. *Journal of Geophysical Research: Biogeosciences*, *119*(5), 741–757. https://doi.org/10.1002/2012jg002230

Zhang, T., Li, J., Pu, J., & Yuan, D. (2019). Carbon dioxide exchanges and their controlling factors in Guijiang River, SW China. *Journal of Hydrology*, *578*, 124073. https://doi.org/10.1016/j.jhydrol.2019.124073

Zhang, Y., Jiang, Y., Yuan, D., Cui, J., Li, Y., Yang, J., & Cao, M. (2020). Source and flux of anthropogenically enhanced dissolved inorganic carbon: A comparative study of urban and forest karst catchments in southwest China. *Science of the Total Environment*, *725*, 138255. https://doi.org/10.1016/j.scitotenv.2020.138255

Zhang, Z., Jia, W., Zhu, G., Shi, Y., Yang, L., Xiong, H., et al. (2021). Hydrochemical characteristics and ion sources of river water in the upstream of the Shiyang River, China. *Environmental Earth Sciences*, *80*(18), 614. https://doi.org/10.1007/s12665-021-09793-2

Zhao, C. (2023). The data of water chemical parameters in Yangtze River (Vision 3.0) [Dataset]. Zenodo. https://doi.org/10.5281/zenodo.8273583

Zhao, M., Sun, H., Liu, Z., Bao, Q., Chen, B., Yang, M., et al. (2022). Organic carbon source tracing and the BCP effect in the Yangtze River and the Yellow River: Insights from hydrochemistry, carbon isotope, and lipid biomarker analyses. *Science of the Total Environment*, *812*, 152429. https://doi.org/10.1016/j.scitotenv.2021.152429

Zhao, Z., Huang, C., Meng, L., Lu, L., Wu, Y., Fan, R., et al. (2021). Eutrophication and lakes dynamic conditions control the endogenous and terrestrial POC observed by remote sensing: Modeling and application. *Ecological Indicators*, *129*, 107907. https://doi.org/10.1016/j.ecolind.2021.107907

Zhong, J., Li, S. L., Ding, H., Lang, Y., Maberly, S. C., & Xu, S. (2018). Mechanisms controlling dissolved CO_2 over-saturation in the Three Gorges Reservoir area. *Inland Waters*, *8*(2), 148–156. https://doi.org/10.1080/20442041.2018.1457848

Zhong, J., Li, S.-L., Ibarra, D. E., Ding, H., & Liu, C.-Q. (2020). Solute production and transport processes in Chinese monsoonal rivers: Implications for global climate change. *Global Biogeochemical Cycles*, *34*(9), e2020GB006541. https://doi.org/10.1029/2020gb006541

Zhong, J., Li, S. L., Zhu, X., Liu, J., Xu, S., Xu, S., & Liu, C. Q. (2021b). Dynamics and fluxes of dissolved carbon under short-term climate variabilities in headwaters of the Changjiang River, draining the Qinghai-Tibet Plateau. *Journal of Hydrology*, *596*, 126128. https://doi.org/10.1016/j.jhydrol.2021.126128

Zhong, J., Wallin, M. B., Wang, W., Li, S. L., Guo, L., Dong, K., et al. (2021a). Synchronous evaporation and aquatic primary production in tropical river networks. *Water Research*, *200*, 117272. https://doi.org/10.1016/j.watres.2021.117272

References From the Supporting Information

Stock, B. C., Jackson, A. L., Ward, E. J., Parnell, A. C., Phillips, D. L., & Semmens, B. X. (2018). Analyzing mixing systems using a new generation of Bayesian tracer mixing models. *PeerJ*, *6*, 1–27. https://doi.org/10.7717/peerj.5096